May 2019

Corrosion Behavior of H-Pile Steel in Different Soils

Ling Ding
Clemson University, dingling1991@gmail.com

CORROSION BEHAVIOR OF H-PILE STEEL IN DIFFERENT SOILS

A Dissertation
Presented to
the Graduate School of
Clemson University

In Partial Fulfillment
of the Requirements for the Degree
Doctor of Philosophy
Civil Engineering

---

by
Ling Ding
May 2019

Accepted by:
Dr. Amir Poursaee, Committee Chair
Dr. Prasad Rao Rangaraju, Co-Chair
Dr. Ronald D. Andrus
Dr. Brandon Ross

ABSTRACT

This dissertation aimed to study the corrosion performance of carbon steel in different soils, collected from the state of Wisconsin. Carbon steel specimens (as-received) as well as steel embedded in mortar (steel-mortar) specimens, to simulate the realistic H-pile design in bridges, were used in this investigation. Both as-received steel and steel-mortar specimens were embedded in as-received soils, with different physiochemical properties, i.e. pH, moisture content, resistivity, chloride content, sulfate and sulfite contents, and the mean total organic carbon concentration, for more than one year. Both specimen types were also embedded in the same as-received soils, but with increased chloride content to 3% by weight of chloride ions for more than one year. In addition, the surface of three identical as-received specimens was modified using the sandblasting method for 5 minutes. These specimens were embedded in one of the collected soils. Different electrochemical measurements were conducted on the specimens to evaluate the corrosion activity of the steel in these soils.

The results showed a comparable corrosion activity of the steel-mortar specimens in all soils compared to the as-received specimens in the same soil both with and without chlorides, except for soils collected from Wausau. No correlation between the available physiochemical data and the observed results was determined. No information on the type and population of the bacteria in the collected soils was available. Perhaps, this information could explain the observed results. In all cases, there was a galvanic current

flowing between specimens in chloride-free and chloride contaminated soils. In addition, corrosion potential values of all specimens remained relatively stable both before and after addition of chlorides, suggesting just measuring the corrosion potential may not be an efficient method to monitor the change of corrosion behavior of steel in the soil. The results of electrochemical experiments also showed significant improvement in corrosion resistance of sandblasted specimens compared to the as-received specimens.

DEDICATION

I dedicate this dissertation to Chang, my grandparents, parents for their love and support all these years.

ACKNOWLEDGMENTS

I would like to express my deepest gratitude to my advisor, Dr. Amir Poursaee for giving me the opportunity to work with him and learn from him. I am truly grateful for his guidance and support. I would like to thank my co-advisor, Dr. Prasad Rao Rangaraju for his assistance and advice throughout this research. I would also like to thank Dr. Ronald D. Andrus and Dr. Brandon Ross for serving on my examination committee.

I would like to thank my Family. They always understand and support me with a lot of patience. They are the power of my study.

The completion of this research would not have been possible without the assistance of my fellow researchers. I want to thank Hamidreza Torbati Sarraf and Trent Dellinger.

This research was funded through the Wisconsin Highway Research Program by the Wisconsin Department of Transportation and the Federal Highway Administration under Project 0092-16-03. The contents of this research reflect the views of the authors who are responsible for the facts and accuracy of the data presented herein. The contents do not necessarily reflect the official views of the Wisconsin Department of Transportation or the Federal Highway Administration at the time of publication.

TABLE OF CONTENTS

Page

LIST OF TABLES

LIST OF FIGURES

Figure Page

CHAPTER 1

1. INTRODUCTION

1.1. Problem Statement

On September 25, 2013, Pier 22 of the Leo Frigo Bridge near Green Bay, Wisconsin, moved vertically approximately 2 feet. This vertical movement reduced structural capacity due to the loss of the section of the steel H-piles that supported the pier (Becker and Rudat 2014). The main reason for such movement was attributed to the severe corrosion of the pile (Becker and Rudat 2014). To understand the corrosion activity of the steel in a similar situation and to provide a framework for service life prediction of such structures, soil samples were collected from different regions of the state of Wisconsin. The laboratory corrosion measurements were conducted on the steel specimens with similar chemical composition used to make the steel piles (according to ASTM A572-50 (Halim, Watkin et al. 2012)) in the collected soils samples. In addition, since concrete is usually cast over the steel pile, laboratory specimens containing steel embedded in mortar, to simulate real field condition, were prepared and their corrosion activities were examined in the laboratory. Besides, the surface of as-received steel was sandblasted for 5 minutes and their corrosion activity in one of the soils was compared to that of the as-received steel specimens in the same soil. The potential for the galvanic corrosion between specimens in as-received soils and soils with elevated chloride content was also evaluated.

1.2. Objective and Dissertation Organization

The objective of this work is to evaluate the corrosion activity of the steel used in the H-piles in soil samples collected from locations with different physicochemical parameters, as well as to develop guidelines for future investigation procedures for evaluating potential pile corrosion in the project design stage. Steel specimens with the same composition used in the H-piles used in this investigation. Since concrete is cast over the steel pile, steel-mortar specimens were prepared and used in this study along with the as-received steel specimens to simulate this configuration.

This study aims to investigate the following:

1. Corrosion activity of as-received steel and steel-mortar specimens in as-received soil samples.
2. Corrosion activity of as-received steel and steel-mortar specimens in soil samples with elevated chloride content.
3. The galvanic effect between as-received steel specimens in as-received soils and soils with elevated chloride content.
4. The impact of connecting the old steel with new steel on the corrosion activity of steel to simulate the corrosion of the repaired structures.
5. The impact of the sandblasting on the corrosion activity of steel in the soil.
6. The impact of temperature on the corrosion activity of steel in the soil.

To understand the corrosion activity of the steel in a similar situation and to provide a framework for service life prediction of such structures, soil samples were collected from nine locations of different regions of the state of Wisconsin. The laboratory corrosion measurements were conducted on the steel specimens with similar chemical composition used to make the steel piles according to ASTM A572-50 (Halim, Watkin et al. 2012) in the collected soils samples. In addition, since concrete is usually cast over the steel pile, laboratory specimens containing steel embedded in mortar, to simulate real field condition, were prepared and their corrosion activities were examined in the laboratory. Ding and Poursaee reported the improvement in corrosion resistance of the sandblasted steel bars in concrete pore solution (Ding and Poursaee 2017). Nevertheless, no study was conducted on the impact of sandblasting of steel on its corrosion behavior in soil. Thus, the surfaces of as-received steel specimens were sandblasted for 5 minutes and their corrosion activity in one of the soils was compared to those for the as-received steel specimens in the same soil. To study the impact of the chloride content of the soil on the corrosion of steel, the chloride content of the as-received soils was increased to 3 wt% and the corrosion of the steel specimens was investigated on these soils as well. The potential for the galvanic corrosion between specimens in as-received soils and soils with elevated chloride content was also evaluated.

1.3. Content of the Dissertation

The content of this dissertation is divided into 6 chapters.

CHAPTER 1 provides an introduction to the dissertation, as well as the objectives and organization of the content.

CHAPTER 2 provides background and literature review, which includes a description of corrosion and metals and corrosion of steel in the soil.

CHAPTER 3 presents the study of corrosion performance of carbon steel in different soils, collected from the state of Wisconsin.

CHAPTER 4 presents the study of generalized regression neural network (GRNN) model, which is used to predict the corrosion potential values and corrosion current densities of ASTM A572-50 steel specimens embedded in nine soils with different physiochemical properties, i.e. pH, moisture content, resistivity, chloride content, sulfate and sulfite contents, and the mean total organic carbon concentration.

CHAPTER 5 presents the study of the influence of time of sandblasting, as a surface mechanical attrition treatment method, on the corrosion behavior of carbon steel in different solutions with different pHs.

CHAPTER 6 provides a summary and recommendations for future work.

CHAPTER 2

2. BACKGROUND AND LITERATURE REVIEW

2.1. Background

Steel H-piles are widely used in bridge structures to resist vertical and lateral loads. Steel H-pile is manufactured from a variety of materials including carbon steel. While carbon steel is susceptible to corrosion, it is widely used due to its low cost and high strength. However, corrosion of the steel piles is often of concern (Wong and Law 1999, Wong 2001, Fleming, Weltman et al. 2008, Becker and Rudat 2014, Wang, Qi et al. 2016). The factors that influence corrosion in the soil are numerous such as soil type, moisture content, the position of the water table, soil resistivity, soluble ion content, soil pH, oxidation-reduction potential and the role of micro-organisms in the soil (Benmoussat and Hadjel 2005).

The most recent severe steel pile corrosion was observed in Pier 22 for the Leo Frigo Bridge (B- 05-381) near Green Bay, Wisconsin. On September 25, 2013, Pier 22 for the Leo Frigo Bridge moved vertically downward approximately 2 feet. This vertical movement reduced structural capacity due to the loss of the section of the steel H-piles that supported the pier (Becker and Rudat 2014). The main reason for such movement was attributed to the severe corrosion of the pile in that location (Becker and Rudat 2014). The investigation determined that several unusual factors changed the environment that led to the severe

corrosion of the steel pile foundation supporting Pier 22. The first factor was the presence of industrial porous fly ash fill in the upper layer of soil in contact with the piles and the second factor was that the water and soils surrounding the pile sections embedded in the fly ash fill contained high concentrations of chloride ions. The porous fly ash contained high levels of sulfates, was frequently moist along sections of the piles and was porous enough to permit relatively free passage of oxygen to the surface of the piles. The combination of these factors caused rapid corrosion of sections of the embedded piles, which led to the crushing/buckling of the most heavily deteriorated sections of the pile. Significant loss in the thickness and width of the pile flanges was observed around and within the collapsed region of each pile. The most significant corrosion damage and greatest section loss were reported in the region that was 1 to 2-1/2 feet above and below the failed region. Pitting corrosion was also observed, specifically in the vicinity of the failed region.

2.2. Corrosion of Metals

Corrosion in metals is caused by the flow of electrons from one metal to another or from one location to another on the surface of the same piece of metal (Fontana 2005). A corrosion cell must exist in order for corrosion to take place. The formation of a corrosion cell requires the presence of an anode and a cathode, an electrical connection between the anode and the cathode, and an electrolyte. Once these conditions are met, an electric current flows and metal is consumed at the anode (Wang, Sweikart et al. 2003).

The potential difference between the anode and the cathode results in the migration of electrons and/or ions from the anode to the cathode along the connection between the anode and cathode while current flows from cathode to anode (Reiser, Bregoli et al. 2005). At the anode, electrons are lost leaving positively charged atoms combine with negatively charged ions. For example, When the anode is iron, the corrosion reaction at the presence of water and oxygen are (Bentur, Berke et al. 1997):

Anode reaction: $Fe^{2+} + 2e^{-} \rightarrow Fe$ (2.1)

Cathode reaction: $O_2 + 2H_2O + 4e^{-} \rightarrow 4OH^{-}$ (2.2)

The mass loss of the metal can be related to the current flow using the Faradays' law (Poursaee 2011) and it is directly proportional to the current flow. Thus, the severity of corrosion is directly related to the amount of current flow.

2.3 Corrosion of Steel in Soil

2.3.1 Soil Properties

Corrosion is one of the leading causes of failures of buried or embedded steel elements in soils such as bridges, pipelines, and tunnels in the United States and worldwide (Ricker 2010). Corrosion of buried metallic structures in soils is also a great issue for safety and economy concern in various industrial applications, e.g. oil/gas, water, sewerage

distribution systems (Yan, Sun et al. 2014). The locally severe corrosion of steel bridge H-piles near pile cap due to corrosive soil caused one portion of the Leo Frigo Bridge, Wisconsin, moving downward vertically 2 feet on Sep. 2013. This movement ultimately led to a total cost of over $20 million (Wang, Qi et al. 2016).

Soil can be considered as a heterogeneous system of pores with colloidal characteristics. The space between the soil particles can be filled with water or gas (Chatterjee, Lal et al. 2009). The corrosive nature of the soil can be considered as the capacity of this environment to produce and to develop the corrosion on a metal, particularly steel (Ferreira, Ponciano et al. 2007). The study of the soil as a corrosive environment is necessary due to the large number of buried infrastructure facilities, such as pipelines, tanks, and H-piles, as their deterioration can represent a significant economic and environmental problem through the years. Nevertheless, the soil, when compared with the other environments such as atmosphere or seawater, is difficult to be classified for potential corrosivity due to its complexity (Ferreira and Ponciano 2006). Acidification, salinity, organic and nutrient depletion, compaction, chemical contamination, landslides, and erosion are all forms of soil degradation that can result from inappropriate land use practices and may lead to premature corrosion of the embedded steel structure in the soil (Oldeman, Hakkeling et al. 1990).

Corrosion of the steel in soil is governed by the principles of electrochemistry (Saji 2010). In low-resistivity soils with different physicochemical properties, such as composition and

different moisture content, the formation of the macro-cells is possible. Sharp changes in oxygen concentration in the soil along the surface of the buried metal structures may lead to different electrical potential, which produces current. The amount of current and its distribution over the surface of the metal depend on the resistivity of the soil and its polarization characteristics. The latter determined by the degree of oxygen penetration of the soil, chloride and moisture content, granulation, and other physicochemical properties of the soil (Cole and Marney 2012).

Soils are classified according to their grain size distribution range. According to the American Association of State Highway and Transportation Officials (AASHTO), soils are been classified into two broad categories. Coarse-grained soils that are gravelly and sandy in nature with less than 50% passing through the No. 200 sieve. Fine-grained soils are with 50% or more passing through the No. 200 sieves. The American Association of State Highway and Transportation Officials (AASHTO) is now almost universally accepted, according to their classification, the gravel particle grain size range from 76.2 to 4.75 mm, sand particle grain size range from 4.75 to 0.075 mm and fines particles such as silts and clays have a grain size less than 0.07 mm (Soil and Rock 2011). Clay soil is very plastic by nature; it becomes sticky and impervious when saturated with water. It has more packed particles and less pore capacity for moisture and oxygen diffusion compared to the other types of soils, meaning it has poor drainage and aeration. Sand and gravel have more drainage and aeration.

In relation to the physical properties of soil, volume shrinkage is the tendency of the soil to start cracking on drying and they swell when wet. When clay/silt soil dries, it forms cracks that allow diffusion of oxygen to the pile and hence the susceptibility of a buried pile to corrosion increases. Because of the poor drainage in clay and silt, the capillary pores of these soils hold a considerable amount of water. The moisture in highly conductive soils indicates high ion content and the possibility of very active corrosion attack (Fontana 2005).

2.3.2. Consequences of Pile Corrosion

Buried steel structures, such as H-piles, are frequently suffered from corrosion due to their direct contact with corrosive soils, resulting in high maintenance cost and even leading to catastrophes in some cases (Wang, Qi et al.). The corrosion of steel piles results in a reduced cross-sectional area of the pile and therefore decreased axial and lateral capacity. Resistivity and acidity are two parameters widely accepted for characterizing the soil corrosively, but they do not often correlate directly to the soil corrosivity or corrosion rate of the buried steels (Pritchard, Hallett et al. 2013, Beben 2014, Fonseca, Niculita et al. 2015).

Decker et al. reported that a section loss of 25% is considered serious for a pile (Decker, Rollins et al. 2008). However, Trungesvik concluded that loss in pile capacity due to corrosion may be greater than generally assumed from the loss of section area (Trungesvik

1976). In his work, a 25% reduction in strength was reported when a corroded specimen having a section loss of 13.6%.

2.3.3. Factors Influencing Steel Corrosion in Soils

Although various parameters on metallic corrosion in soils have been widely studied, such as electrical resistivity, pH, water content, redox potential, ionic species, salinity, microbial activities, soil texture, porosity and other physical factors (Moore and Hallmark 1987, Chaker 1989, Liu, Wu et al. 2010, Yan, Sun et al. 2014), some soil properties affecting corrosion are still not fully understood due to the complexity of the soil medium. It has been established that corrosion of ferrous materials in soils depends primarily on the soil properties rather than the kind of ferrous material (Denison and Hobbs 1934). Generally, soils with high resistivity, high dissolved salt, and high acidity are more aggressive towards metallic materials.

Several environmental conditions may act individually or in complex relationships to influence the corrosion rates of the buried steels. Many of these variables are highly dependent upon each other and the properties of the buried steels. Robinson defined many physical and chemical characteristics that can determine the soil corrosivity as oxygen concentration, the presence of sulfate and sulfide ions, resistivity, total acidity, redox potential and others (Robinson 1993). In agreement with the parameters cited above, Fitzgerald studied how the corrosivity of the soil is influenced by oxygen content, dissolved salts, pH, elements that form acids, the concentration of chloride, sulfide, and sulfate,

resistivity, total acidity, redox potential, and others, depending on the specific application (Fitzgerald 1993). In addition, dissimilar metals in contact with each other, different soils in contact with the structure, different aeration, steel embedded in concrete and soil and connection between old and new steel pieces are the other factors influencing the corrosion behavior of the buried steel.

2.3.3.1. Resistivity

Resistivity, the reciprocal of conductivity, indicates the ability of an environment to carry corrosion currents. A soil's resistance (R) to the passage of electricity is the property of the soil that is an indicator of the severity of the corrosion measured in ohm-cm, the resistivity can vary from 30 ohm-cm in seawater to in excess of 100,000 ohm-cm in dry sand or gravel. The AWWA (American Water Works Association) formula considers less than 700 ohm-cm to be severely corrosive, while the steel-line industry considers anything less than 1000 ohm-cm to be "very severely corrosive" (Chaker 1989). Resistivity is a function of the soil moisture and the concentration of current-carrying solution ions.

In general, the potential for metallic corrosion was thought to be more severe in moist fine-grained soils with low resistivity (<1,000 – 3,000 Ω cm) and extreme pH (<5 or >10.5) compared to other conditions (Peabody 1967, Roberge 2000). Table 2.1 summarizes the soil corrosivity based on soil resistivity.

Table 2. 1. Corrosion severity ratings based on soil resistivity.

Soil resistivity (Ω.cm)	Corrosivity rating
>20,000	Essentially noncorrosive
10,000 – 20,000	Mildly corrosive
5,000 – 10,000	Moderately corrosive
3,000 – 5,000	Corrosive
1,000 – 3,000	Highly corrosive
< 1,000	Extremely corrosive

2.3.3.2. pH

pH is the measure of the soil's alkalinity or acidity, which is the logarithm of the reciprocal of hydrogen concentration. pH measurements may be useful in identifying unusual soil conditions but in most cases are only significant in distinguishing between otherwise similar soils. ASTM test method for pH of soils for use in corrosion testing (G 51-77) indicates that soil pH should be measured in situ or immediately after a sample is removed from the field. The pH of the soil was considered as the factor most affecting underground corrosion since it was discovered. However, previous studies showed otherwise. Penhale buried steel plates in 33 different soils for 20 years (Penhale 1984). For each soil, both the pH and total acidity were measured, and no correlation was found between total acidity and corrosion rate. Rajani and Maker examined the corrosion rates of cast iron pipes obtained under various pH conditions of pipes, working on an American Water Works Association-funded project on the methodology for estimating remaining service life (Rajani and Makar 2000). Based on their data, no correlation was observed between the pH and the pitting rates. Doyle et al. compared the results of pH testing with the corrosion rates of samples from 98 sites in Ontario, Canada, and found no correlation (R^2=0.04)

between pH and corrosion rates (Doyle, Seica et al. 2003). Thus, it can be concluded that the pH has little relationship with the corrosion rate and the pH alone is a poor indicator of corrosion in buried conditions.

2.3.3.3. Chlorides

Elias and Christopher identified high concentrations of sulfates (>200 pm) and chlorides (>100 ppm) as indicatives of corrosive soil in Federal Highway Administration (FHWA) guidelines for mechanically stabilized earth (MSE) wall fill (Elias and Christopher 1997). Chloride ions are generally harmful, as they participate directly in anodic dissolution reactions of metals. Also, their presence tends to decrease soil resistivity. Chlorides may occur naturally in soils as a result of brackish groundwater and historical geological seabeds. Chlorides may also come from external sources such as de-icing agents applied to road surfaces (Roberge 2000). Wong and Law suggested that the potential for pile corrosion may be significantly less than that for buried pipelines and that the rate of pile corrosion may not be influenced by the same factors that govern corrosion of buried pipelines (Wong and Law 1999). The decomposed granite at the side they studied was considered as an undisturbed natural soil. The results of the studies by Romanoff (Romanoff 1970) show that corrosion of the steel piles in undisturbed soils is very small. Since it is commonly agreed that oxygen and water have to be readily available in order for a corrosion process to be sustained, there should be no difference in a corrosion process between a sedimentary and a residual soil.

2.3.3.4. Sulfides

Most soils will show at least a trace of sulfides and/or sulfates, and this only may be significant in conjunction with the relevant redox potential (< + 100 mV). Sulfate levels are of more significant where concrete structures are concerned (Palmer 1989).

2.3.3.5. Chemical Composition of Soil

Chemical composition plays a key role in understanding how soil influences the corrosion of buried steel. The chemical compositions of soil usually include NaCl, $CaCl_2$, $MgCl_2$, KCl, $NasSO_4$, $NaHCO_3$, and $NaNO_3$. The chemical elements that are responsible for causing corrosion are sodium, potassium, calcium, and magnesium, and others are acid-forming elements, such as carbonates, bicarbonates.

2.3.3.6. Moisture Content

The moisture content of soils plays a major role in the corrosion of buried ferrous metals until a limit is reached, where a decline in corrosion rates takes place. Several researchers have investigated the effect of moisture content on the corrosion of buried ferrous metals. For example, Gupta and Gupta (Gupta and Gupta 1979) performed a series of laboratory tests on steel specimens exposed in soils taken from three locations in India. The soil types of the three sites used in these tests were sandy, sandy loam and loamy. Mild steel test specimens 50 mm × 25 mm × 1.6 mm were burnished with emery cloth, decreased with toluene and weighed. All the three soils were oven-dried at 105 °C before the test. After 6 months, the metal coupons were taken out, cleaned and weighed for mass loss

measurement. In another study related to the corrosion of pipes in soils, Noor and Al-Moubaraki examined the effect of moisture content on the corrosion behavior of X60 steel in soils of different cities in Saudi Arabia at ambient temperature (29 ± 1°C) (Noor and Al-Moubaraki 2014). The corrosion rate of X60 steel in each soil was found to increase with increasing soil moisture content up to a maximum value of 10% and then decreased with further increase in moisture content.

2.3.3.7. Bacteria in Soil

Microbiologically Influenced Corrosion (MIC) is defined as the change in the corrosion behavior of material/metal in the presence of micro-organisms (Costerton, Cheng et al. 1987, Hubert, Nemati et al. 2005, Enning, Venzlaff et al. 2012). Bacteria are attached to the metal surface and form biofilm (Costerton, Cheng et al. 1987), which degrades the metal surface by changing its physical and chemical characteristics due to the biochemical activities associated with their metabolism, growth, and reproduction (Hamilton 1985). MIC is an electrochemical corrosion influenced by the presence/action of biological agents such as, but not limited to, bacteria. One of the key elements of MIC is sulfate-reducing bacteria (SRB). SRB are anaerobic bacteria that can be found in oxygen-deficient saturated soils, with a pH from 6–8, containing sulfate ions, organic compounds, and minerals, and they grow in soils at a temperature of 20–30 °C. SRB are a diverse group of heterotrophic and mixotrophic bacteria (Little, Ray et al. 2000), they are anaerobic; in other words, they do not require oxygen for growth and activity, so as an alternative to oxygen, these bacteria use sulfate with consequent production of sulfide (Javaherdashti 1999).

Perhaps, the key element of understanding how SRB can contribute to corrosion will be understanding the concept of "mixed bacterial communities" or "biofilms". A manifestation of biofilms can be seen as "tubercles" on the surface of metallic surfaces, resulting in localized corrosion (Javaherdashti 2011). Studies showed that on metallic surfaces over time, SRB number on these surfaces increases (Sungur, TÜRETGEN et al. 2010), indicating that a biofilm is formed. Industrial cases where MIC is a problem are usually characterized by a lack of single-type cultures-alternatively pure cultures of one type of bacterium. Actually, even the term "micro-organism" itself refers to a wide range containing bacteria, cyanobacteria, algae, lichens, and fungi (Sand 1997, Setareh and Javaherdashti 2006).

SRB, abundant in soil environments and easily cultured and detected and are known as one of the key microbes in the MIC process (Fauque 1995). During the metabolic process, sulfate is reduced to sulfide. These biogenic sulfides react with hydrogen ions produced by metabolic activities or by cathodic reaction of the corrosion process to form hydrogen sulfide (H_2S). In classical MIC theory, SRB accelerates the removal of cathodic hydrogen by the action of their hydrogenase enzyme, which decreases cathodic overpotential and increases the corrosion rate (cathodic depolarization theory; CDT) (von Wolzogen Kuehr and Van der Vlugt 1964). Biogenic sulfides (or H_2S) further react with dissolved iron to form FeS film on the metal substrate (Videla 1985, Lee and Characklis 1993). Iron sulfides have relatively good electric conductivity, noble electrode potential, and low hydrogen evolution overpotential. Therefore, the galvanic coupling between the FeS film and nearby

metal substrate is set and the corrosion is accelerated. This FeS film is not permanently cathodic toward mil steel (Tiller 1950). The action of SRB is required to maintain the electrochemical activity of FeS. In soil environment, the maximum corrosion rate of steel and iron by the action of SRB is reported to be 0.7 mm/y to 7.4 mm/y (Jack, Rogoz et al. 1994).

CHAPTER 3

3. CORROSION ASSESSMENT OF STEEL IN DIFFERENT SOILS FROM THE STATE OF WISCONSIN

3.1. Introduction

Steel H-piles are widely used in bridge structures to resist vertical and lateral loads. Steel H-pile is manufactured from a variety of materials including carbon steel. While carbon steel is susceptible to corrosion, it is widely used due to its low cost and high strength. However, corrosion of the steel piles is often of concern (Wong and Law 1999, Wong 2001, Fleming, Weltman et al. 2008, Becker and Rudat 2014, Wang, Qi et al. 2016). The factors that influence corrosion in the soil are numerous such as soil type, moisture content, the position of the water table, soil resistivity, soluble ion content, soil pH, oxidation-reduction potential and the role of micro-organisms in the soil (Benmoussat and Hadjel 2005).

Some studies showed that improvement of a metal's mechanical properties can be achieved by alteration of its surface structure (Liu, Wang et al. 2001, Tao, Wang et al. 2002, Chen, Lu et al. 2005, Balusamy, Kumar et al. 2010). Sandblasting was one method used for surface strengthening (Chintapalli, Rodriguez et al. 2014), surface modification (Chintapalli, Marro et al. 2013), surface cleaning and rust removal purposes (Raykowski, Hader et al. 2001). Ding and Poursaee reported the improvement in corrosion resistance of the sandblasted steel bars in concrete pore solution, and they hypothesized that the formation of calcium-rich layer combined with the enhanced passive layer on the

sandblasted specimens were the reasons for the improvement (Ding and Poursaee 2017). Nevertheless, to the best knowledge of the authors, no study was conducted on the impact of sandblasting of steel on its corrosion behavior in soil.

On September 25, 2013, Pier 22 of the Leo Frigo Bridge near Green Bay, Wisconsin, moved vertically approximately 2 feet. This vertical movement reduced structural capacity due to the loss of the section of the steel H-piles that supported the pier (Becker and Rudat 2014). The main reason for such movement was attributed to the severe corrosion of the pile in that location (Becker and Rudat 2014). To understand the corrosion activity of the steel in a similar situation and to provide a framework for service life prediction of such structures, soil samples were collected from different regions of the state of Wisconsin. The laboratory corrosion measurements were conducted on the steel specimens with similar chemical composition used to make the steel piles (according to ASTM A572-50 (Halim, Watkin et al. 2012)) in the collected soils samples. In addition, since usually concrete is cast over the steel pile, laboratory specimens containing steel embedded in mortar, to simulate real field condition, were prepared and their corrosion activities were examined in the laboratory. Besides that, the surface of as-received steel was sandblasted for 5 minutes and their corrosion activity in one of the soils was compared to that for the as-received steel specimens in the same soil. The potential for the galvanic corrosion between specimens in as-received soils and soils with elevated chloride content was also evaluated.

3.2. Steel Specimens

As-received specimens were prepared from carbon steel, satisfying ASTM A572-50, with the chemical composition given in Table 3.1.

Table 3. 1. Chemical composition (%) the steel specimens.

C	Si	Mn	P	S	V	Ni	Co
0.23	0.4	1.35	0.04	0.05	0.06	0.015	0.05

As-received specimens with a length of 101.6 mm (4 in.) and width of 25.4 mm (1 in) were cut and copper wire was spot welded to one end for electrical connection. To prevent extraneous effects, 25.4 mm (1 in.) of one end of each specimen with the wire connection was coated with epoxy, as shown in Figure 3.1(a).

Steel-mortar specimens with a length of 127 mm (steel 76.2 mm (3 in.) and mortar 50.8 mm (2 in.)) as shown in Figure 3.1 (b) were also prepared. The mortar section comprised Type I Portland cement with w/c of 0.45, and 2.5 sand/cement ratio with a maximum aggregate size of 2.36 mm. For each steel-mortar specimen, first mortar was cast as 50.8 mm (2 in.) cubes, then the steel specimen was vertically embedded into the fresh mortar with the length of 25.4 mm (1 in.). Steel-mortar specimens were wet cured for 48 hours and demolded and kept in water for 7 days before being embedded in the soil for electrochemical measurements.

The surface of as-received specimens was treated by particles with an approximately 750 µm diameter under 350 kPa of air pressure. The specimens were sandblasted for 5 minutes. Then 25.4 mm (1 in.) of one end of each specimen with the wire connection was coated with epoxy.

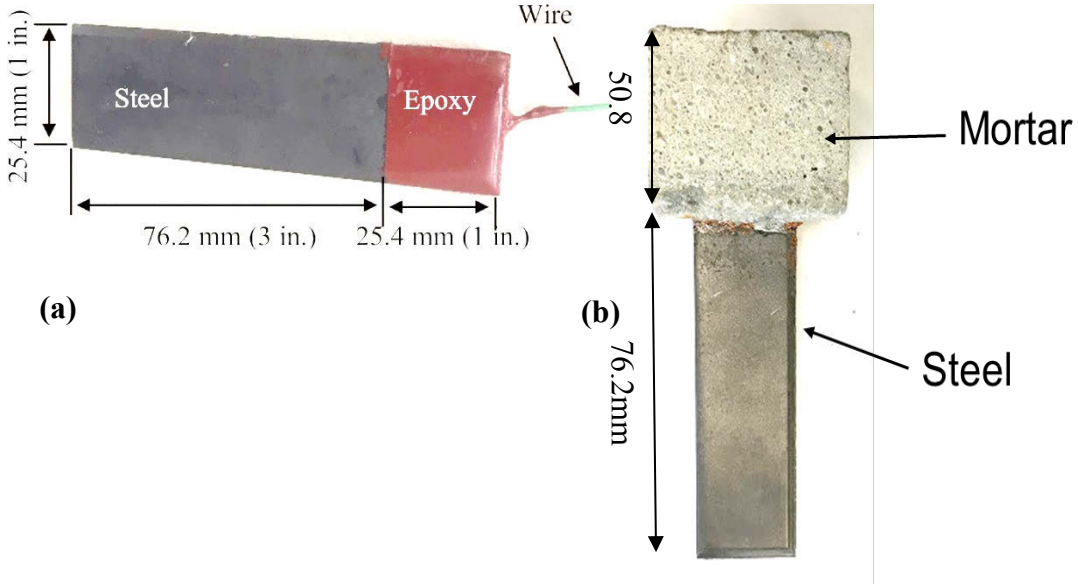

Figure 3. 1. One of the (a) as-received steel specimens and (b) steel-mortar specimens.

3.3. Soil Samples

Soil samples were collected from different locations in the state of Wisconsin, as shown in Figure 3.2. Figure 3.3 shows the pictures of the locations. The physicochemical parameters of the collected soil samples were measured as followings: moisture content according to ASTM D2974-87 (ASTM 2000), pH by using EPA 9054 (EPA 2004), soil resistivity according to EPA 120.1 (EPA 1982), chloride and sulfate contents following

EPA 300.0 (Hautman and Munch 1997), and the total organic carbon using EPA 9060 (EPA 2010). Table 3.2 shows the physicochemical parameters of 9 soil samples in group one. Two groups of the soils was used in this study. The measurement cells in group one were prepared with the as-received soils, while the chloride was added and its content in the soils was adjusted to 3% by weight of the soil in group two.

Figure 3. 2. Locations of the collected soils.

Table 3. 2. Physicochemical parameters of 9 soil samples.

Location	Sample ID	AASHTO Classification	Moisture Content (%)	pH	Resistivity (ohms-cm)	Chloride (w%)	Sulfate (mg/kg)	Sulfide (mg/L)	MTOC* (mg/kg)
Milwaukee	1	A-2-6	22.3	7.80	34300	0.007	33.6	<20.0	25200
	2	A-2-6	22.1	7.80	27700	0.006	34.7	<20.0	8055
Madison	3	A-6	66.9	7.0	1000	0.727	144.0	<20.0	262000
	4	A-6	37.7	6.80	2000	0.210	<31.9	<20.0	31700
	5	A-6	57.9	7.0	1200	0.582	219.0	54.7	37400
	6	A-2-6	32.1	7.90	3200	0.143	<29.2	<20.0	11800
	7	A-2-6	23.6	7.0	5100	0.087	40.3	<20.0	5030
Wausau	8	A-1-b	8.8	6.08	66800	0.014	24.7	<20.0	642
	9	A-1-b	11.3	7.12	38000	0.016	26.2	<20.0	614

* ***Mean Total Organic Carbon***

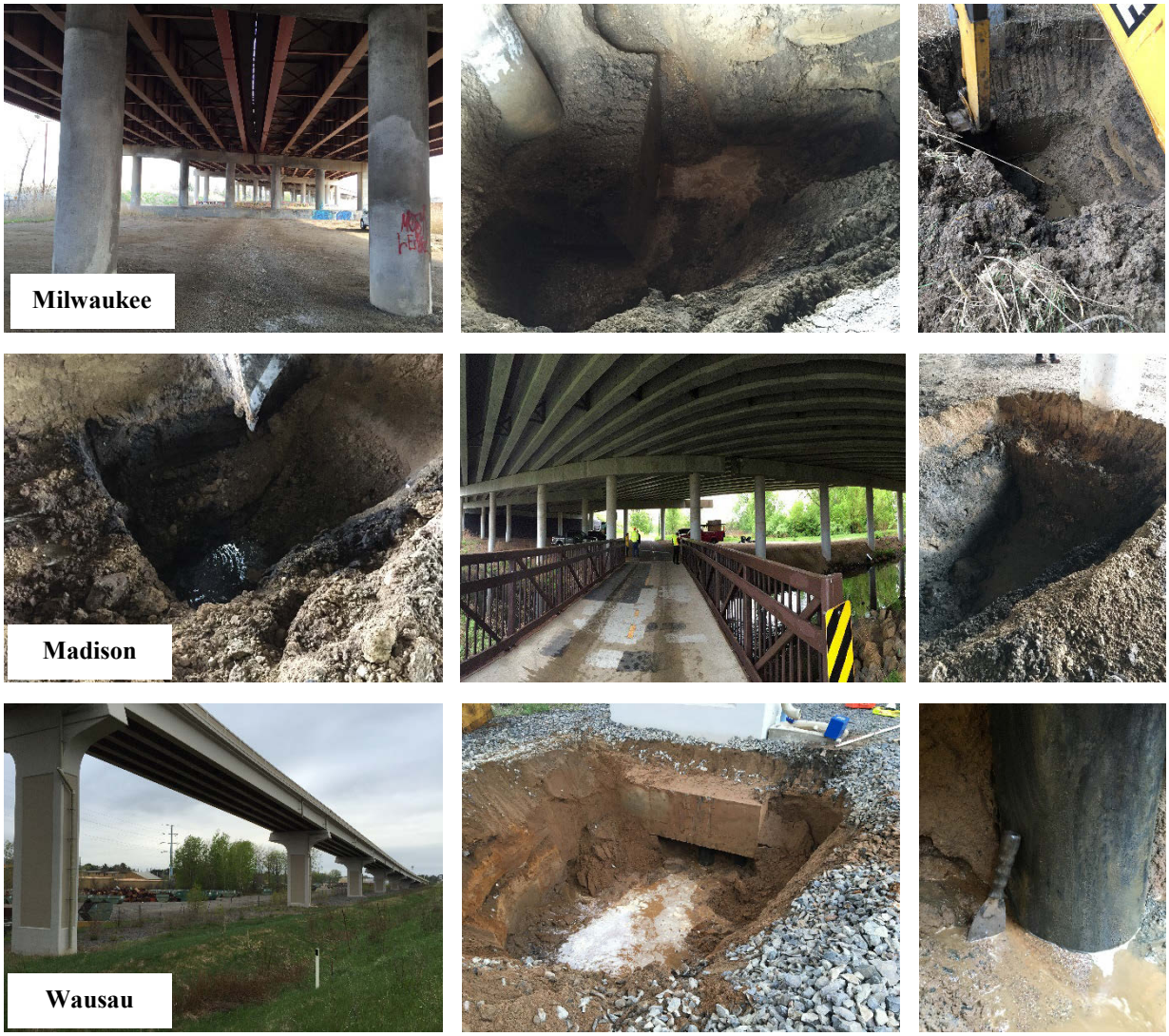

Figure 3. 3. Locations, where the soil samples were collected.

3.4. Experimental methods

For each soil sample (in all groups), a container with three identical specimens, either as-received steel, steel-mortar, or sandblasted steel, was prepared. Just one of the soils, i.e. soil 9, was used for the sandblasted specimens. The specimens were vertically embedded

in soils (for steel-mortar specimens, mortars on top to simulate the real condition) and the container was sealed with a lid to minimize moisture loss.

A three-electrode measurement setup, as shown in Figure 3.4, including a specimen as the working electrode, a saturated calomel electrode (SCE) as the reference electrode, and a 316-stainless steel sheet as the counter electrode, was used for the electrochemical test. To evaluate the probability of the corrosion of the specimens, the corrosion potential of all specimens was measured versus SCE.

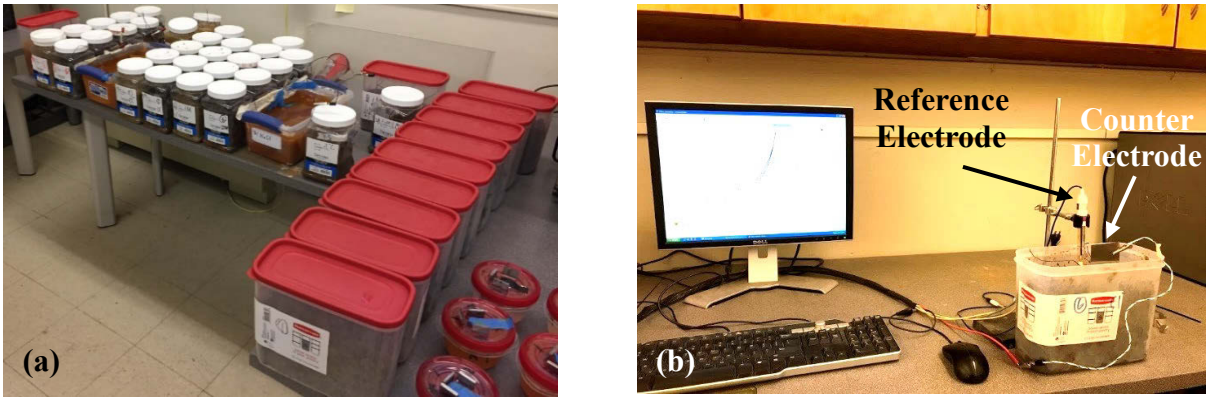

Figure 3. 4. (a) All experiment cells; (b) One of the corrosion measurement cells.

Linear Polarization Resistance (LPR) technique was used to determine the polarization resistance, R_p, of the steel specimens, by applied ±10mV potential over the corrosion potential and measure the resultant current. The LPR and potential measurements were started 24 hours after embedding the specimens in the soil. The cyclic polarization technique was used to evaluate the susceptibility of the specimens to pitting corrosion. For all cyclic polarization tests, the potential scanned from -100 mV against open circuit

potential to +500 mV versus the reference electrode and reversed to -100 mV versus the reference electrode with the scan rate of 0.166 mV/s (ASTM 2004).

It was hypothesized that when two identical steel specimens, one embedded in as-received soil and one in soil with the elevated chloride content, galvanic corrosion was flowed between them. To evaluate this hypothesis, steel specimens were embedded in two separate containers, one filled with as-received soil and the other filled with the same soil, with increased chloride content to 3 weight % of the soil. Specimens were connected together by copper wires. 24 hours before conducting the experiment, the specimens were disconnected from each other; then the galvanic current between them was measured using Zero Resistance Ammetery (ZRA) technique.

The corrosion current density, i_{corr}, can be calculated from the measured R_p from the LPR tests, using the following equation:

$$R_p = B/I_{corr} \quad (3.1)$$

$$i_{corr} = I_{corr}/A \quad (3.2)$$

where B is the Stern-Geary constant and A is the corroded surface area. B can be calculated using eq (3.3):

$$B = \beta_a \beta_{a\,/\,2.3} (\beta_a + \beta_c) \quad (3.3)$$

where β_a and β_c are anodic and cathodic Tafel slopes. To measure these values, Tafel test was conducted on the specimens in each soil by polarizing the steel specimens ±500 mV versus its corrosion potential with a scan rate of 0.166 mv. s^{-1} (ASTM 2004) and measuring the resultant current. The slopes of the linear portions of the potential vs. log of the current curve in each part, i.e. anodic and cathodic, are the β_a and β_c, respectively.

During repair and maintenance of the pile, it is probable to connect new steel to the old corroded one. To study the change in corrosion of steel due to such condition, old and corroded steel was obtained from WisDOT and were connected to the new as-received specimens in a measurement cell with water. Epoxy coating on old rusted specimens provided the same exposure area as as-received specimens and prevented extraneous effects.

3.5. Results and discussion

3.5.1. Corrosion Measurements

Table 3.3 shows the average Tafel slopes and the calculated Stern-Geary constants of the specimens in different soils. These values were used to calculate the corrosion current densities using R_p values obtained from the LPR measurements.

Table 3. 3. Tafel slopes (βa and βc) and calculated Stern and Geary Constants (B).

Soil sample ID	βa	βc	B
1	0.53	0.21	0.03
2	0.31	0.44	0.04
3	0.57	0.51	0.13
4	0.33	050	0.06
5	0.49	0.36	0.06
6	0.38	0.43	0.05
7	0.43	0.34	0.05
8	0.23	0.40	0.02
9	0.38	0.31	0.03

Figures 3.5a and 3.5b show the corrosion potential values of the as-received and the steel-mortar specimens embedded in soils without the addition of chloride, respectively.

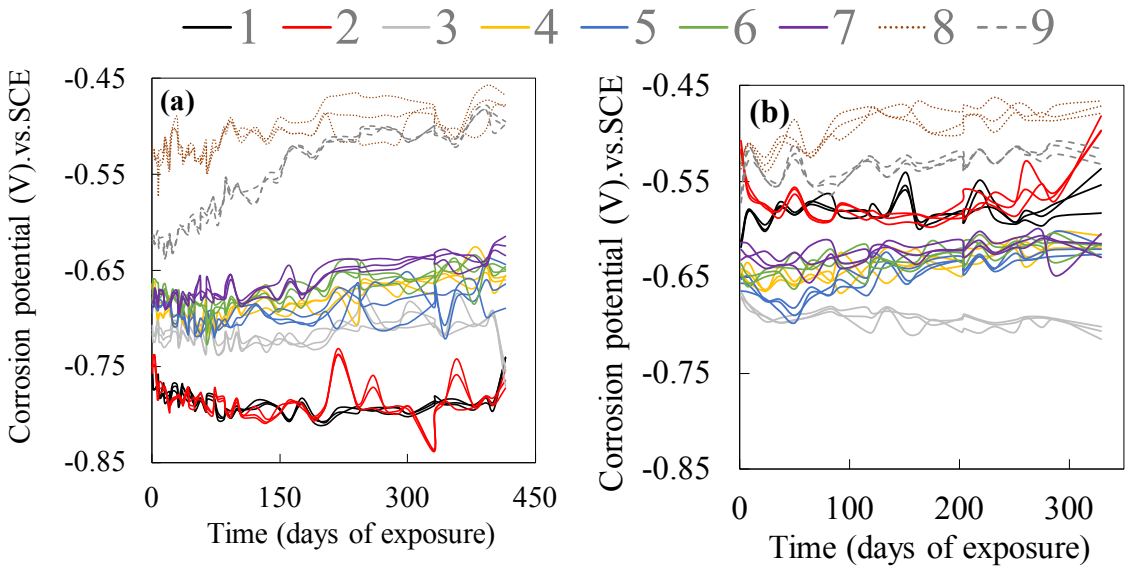

Figure 3. 5. Corrosion potential values of (a) as-received and (b) steel-mortar specimens in 9 different soils (without the addition of Cl).

Figures 3.6a and 3.6b show the corrosion potential values of the as-received and steel-mortar specimens embedded in soils with 3% chloride by weight of soil, respectively.

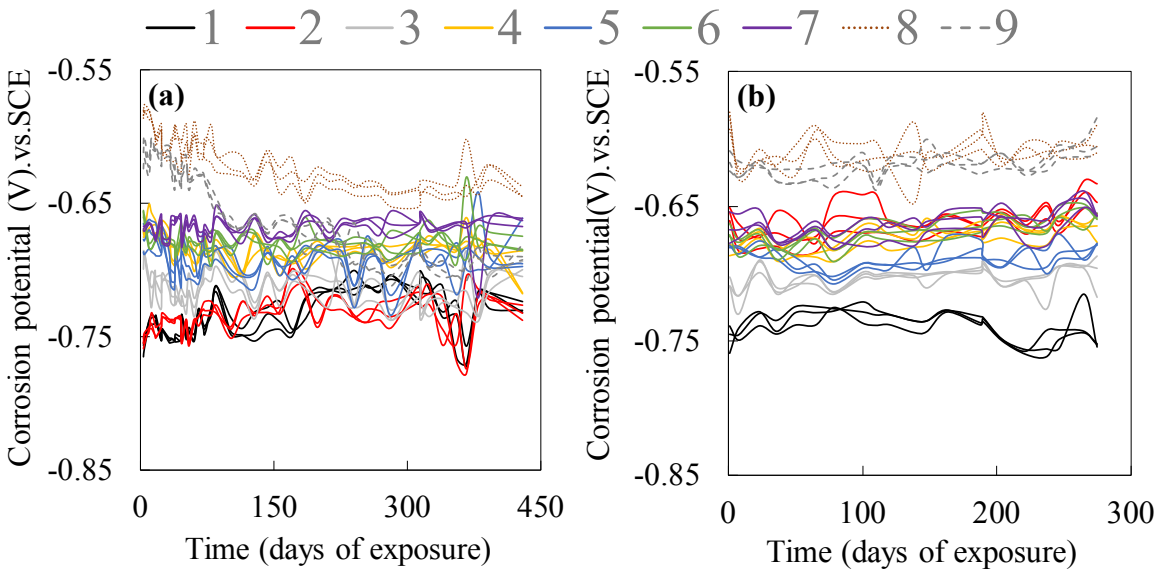

Figure 3. 6. Corrosion potential values of (a) as-received and (b) steel-mortar specimens in 9 different soils (with 3% Cl by weight).

At the end of the experiments, the specimens (both as-received and steel-mortar) were removed from the soils. Then, pictures were taken from both sides of each specimen (Appendix A) and image analysis was carried out with the aid of ImageJ and the corroded surface area on each specimen was measured. Table 3.4 shows the average corroded area for each specimen in different soils.

Table 3. 4. Calculated corroded area of the specimens, after, they removed from the soils.

Soil	As-received		Soil	Steel-mortar	
	Corrode area (m^{-2})			Corrode area (m^{-2})	
	As-received soil	Soil with 3% NaCl		As-received soil	Soil with 3% NaCl
1	8.5×10^{-4}	1.48×10^{-3}	1	3.4×10^{-4}	1.44×10^{-3}
2	6.8×10^{-4}	1.97×10^{-3}	2	3.2×10^{-4}	9.1×10^{-4}
3	2.15×10^{-3}	2.78×10^{-3}	3	2.06×10^{-3}	2.48×10^{-3}
4	1.63×10^{-3}	2.32×10^{-3}	4	1.02×10^{-3}	1.84×10^{-3}
5	1.84×10^{-3}	2.44×10^{-3}	5	1.41×10^{-3}	2.34×10^{-3}
6	1.53×10^{-3}	2.21×10^{-3}	6	6.5×10^{-4}	1.79×10^{-3}
7	1.20×10^{-3}	2.04×10^{-3}	7	4.3×10^{-4}	1.68×10^{-3}
8	1.6×10^{-4}	1.33×10^{-3}	8	1.3×10^{-4}	4.0×10^{-4}
9	1.7×10^{-4}	1.41×10^{-3}	9	2.6×10^{-4}	1.08×10^{-3}

The current destines were calculated, using the corroded areas given in Table 3.4 and the results are shown in Figures 3.7 and 3.8.

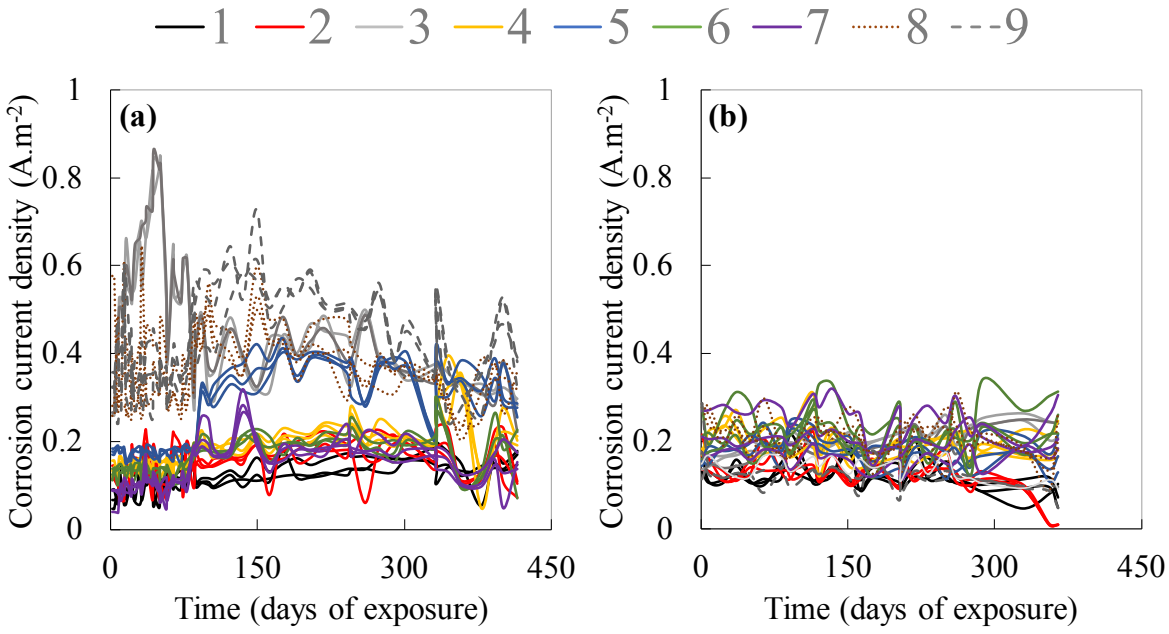

Figure 3. 7. (a) Corrosion current densities of (a) as-received and (b) steel-mortar specimens in 9 different soils (without the addition of Cl).

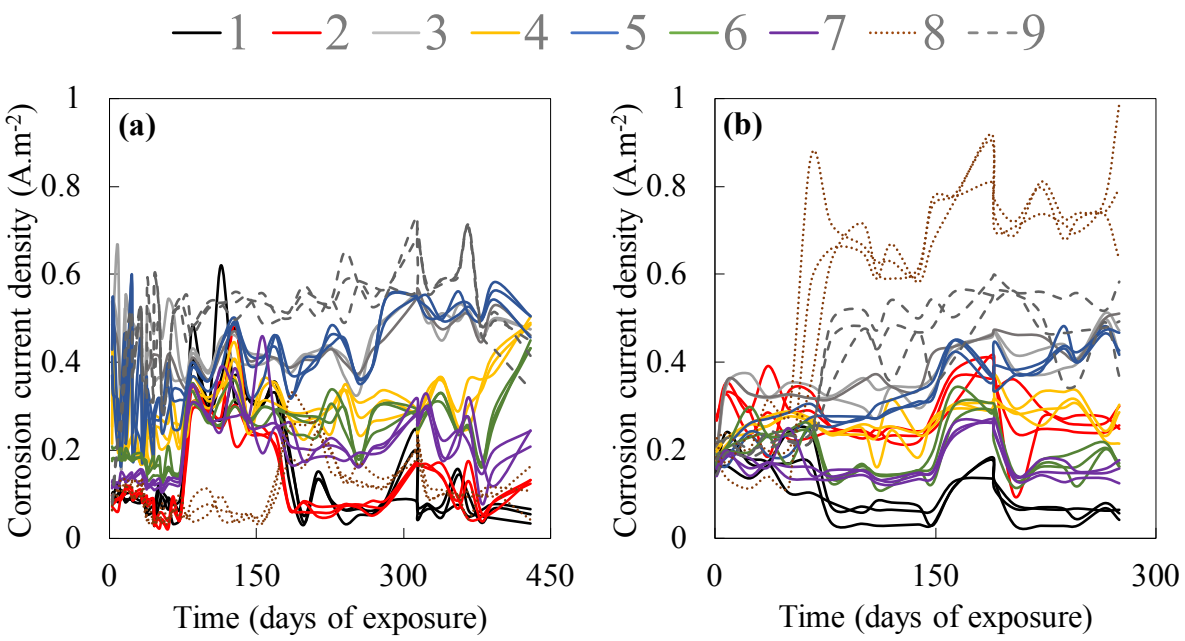

Figure 3. 8. (a) Corrosion current densities of (a) as-received and (b) steel-mortar specimens in 9 different soils (with 3% Cl by weight).

At the end of the experiments, the gravimetric analysis was conducted on all specimens and the weight loss was measured. In addition, the results of the corrosion current density measurements, Figures 3.7 and 3.8, were used to calculate the weight loss during the exposure time using Faraday's law, (Poursaee 2010), the results of the measured and calculated weight loss are shown in Table 3.5 and Figure 3.9 shows the comparison between these values.

Table 3. 5. Average calculated and measured weight loss of the specimens (AR: As-received specimen, SM: Steel-mortar specimen).

Soil	Calculated weight loss (g)				Measured weight loss (g)			
	As-received soil		Soil with 3% Cl		As-received soil		Soil with 3% Cl	
	AR	SM	AR	SM	AR	SM	AR	SM
1	2.15	0.34	4.30	3.97	2.60	0.92	5.53	4.42
2	2.14	0.34	2.78	1.73	2.98	0.94	3.70	2.43
3	7.40	3.29	13.12	6.45	6.76	2.18	10.38	7.00
4	3.39	1.60	7.68	6.38	3.75	1.37	9.60	8.72
5	5.86	2.07	11.21	5.29	4.82	2.00	10.27	6.82
6	2.81	1.16	8.17	7.40	2.47	2.58	9.73	8.97
7	1.98	0.71	6.71	5.92	2.45	0.73	7.19	6.28
8	2.60	1.23	10.62	14.65	3.01	1.95	10.29	15.26
9	3.99	9.28	7.77	16.60	4.99	10.75	10.34	18.73

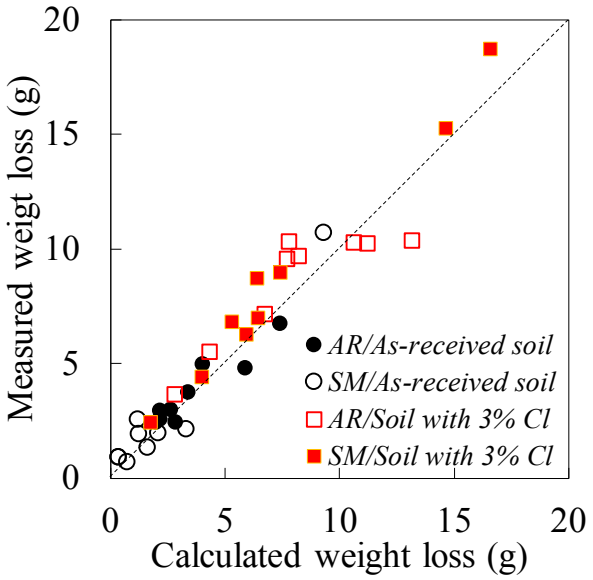

Figure 3. 9. Comparison between the measured and calculated weight loss (AR: As-received specimen, SM: Steel-mortar specimen).

As can be seen, a good agreement exists between the measured and calculated values. The as-received steel specimens in as-received soil 3 showed the highest weight loss compare to the other as-received specimens. However, the steel-mortar specimens in soil 9 had the

highest weight loss compared to the other steel-mortar specimens in both as-received soils and soils with 3% Cl. The high corrosion activity in soil 3 can be attributed to the level of sulfate in that soil (Table 3.2). However, this high corrosion activity was not observed for soil 5, which had the highest sulfate content among all soil samples. It was hypothesized that the bacteria in the soil samples were responsible for such observation. Nonetheless, no data on the type and population of the bacteria were available to support this hypothesis.

To compare the two different types of specimens, the corrosion potentials and corrosion current densities of the steel-mortar specimens, in soils without increasing their chloride content, were plotted against the same values for the as-received steel specimens as shown in Figures 3.10.

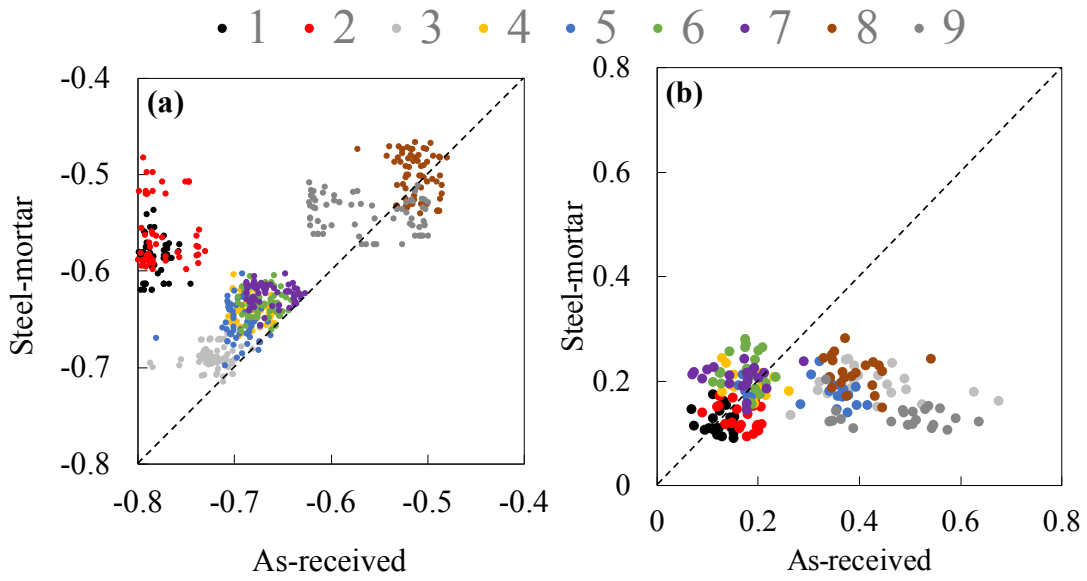

Figure 3. 10. Comparison of (a) corrosion potential values (V) and (b) corrosion current densities ($A.m^{-2}$) between as-received specimens and steel-mortar specimens in 9 different soils (without the addition of Cl).

As can be seen, the corrosion potential values for as-received and steel-mortar specimens were comparable, except for soils 1 and 2. However, in general, the corrosion current densities of the as-received specimens were higher than those for the steel-mortar specimens. It can be concluded that overall, steel-mortar specimens indicated less corrosion activity compared to the as-received steel specimens in the as-received soils.

Comparison of the corrosion current densities and corrosion potential values of as-received steel and steel-mortar specimens in soils with elevated chloride content are shown in Figure 3.11.

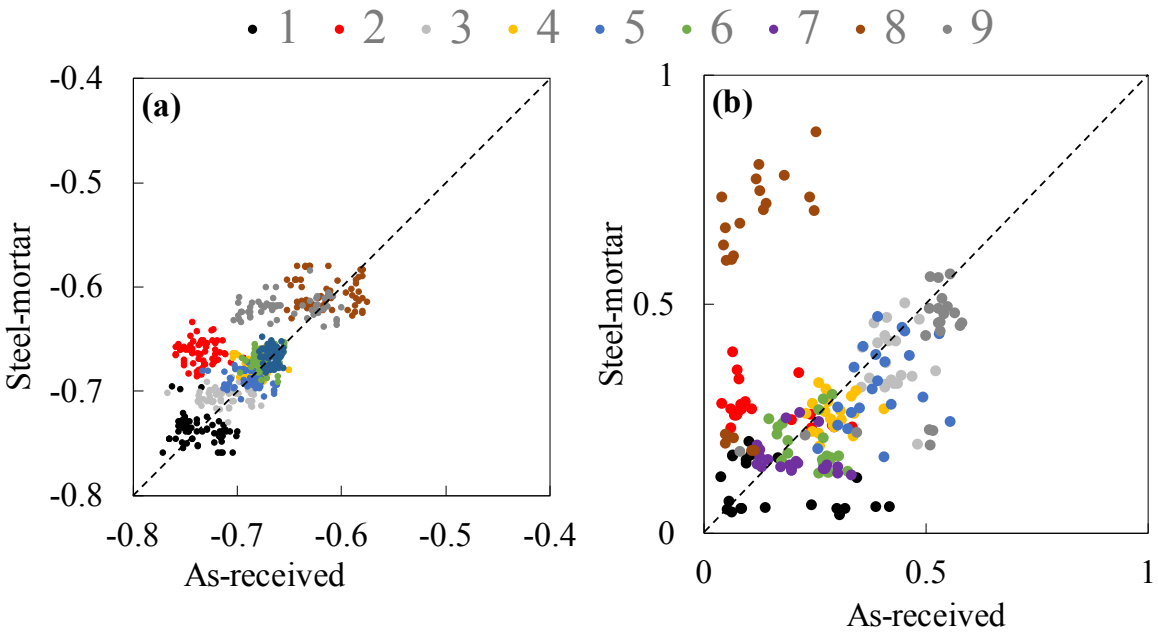

Figure 3. 11. Comparison of (a) corrosion potential values (V) and (b) corrosion current densities ($A.m^{-2}$) between as-received specimens and steel-mortar specimens in 9 different soils (with 3% Cl by weight).

As can be seen, after the addition of chloride, all specimens showed comparable corrosion potential values. The corrosion densities of the steel-mortar specimens were also

comparable, except for soils 8 and 9, which were considerably higher for steel-mortar specimens.

Figures 3.12 and 3.13 show the results of the cyclic polarization experiments on one of the specimens after 2 days and 420 days exposure to as-received soils and soils with the elevated chloride content.

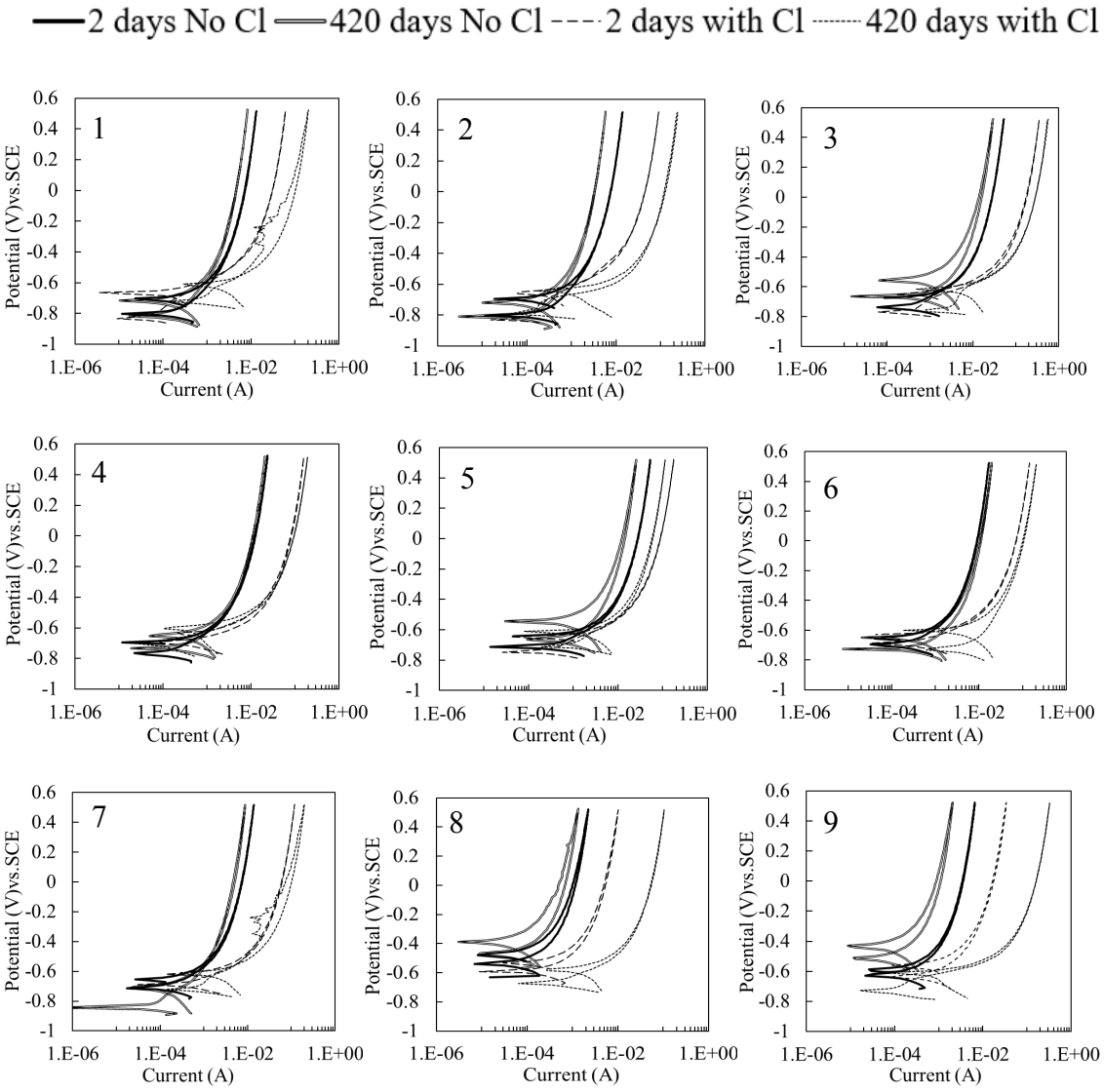

Figure 3. 12. Cyclic polarization plots for one of the as-received specimens in each soil (1 to 9 according to Table 3.2), after 2 days and 420 days exposure to chloride free and 2 days and 420 days exposure to 3% by weight chloride contaminated soils.

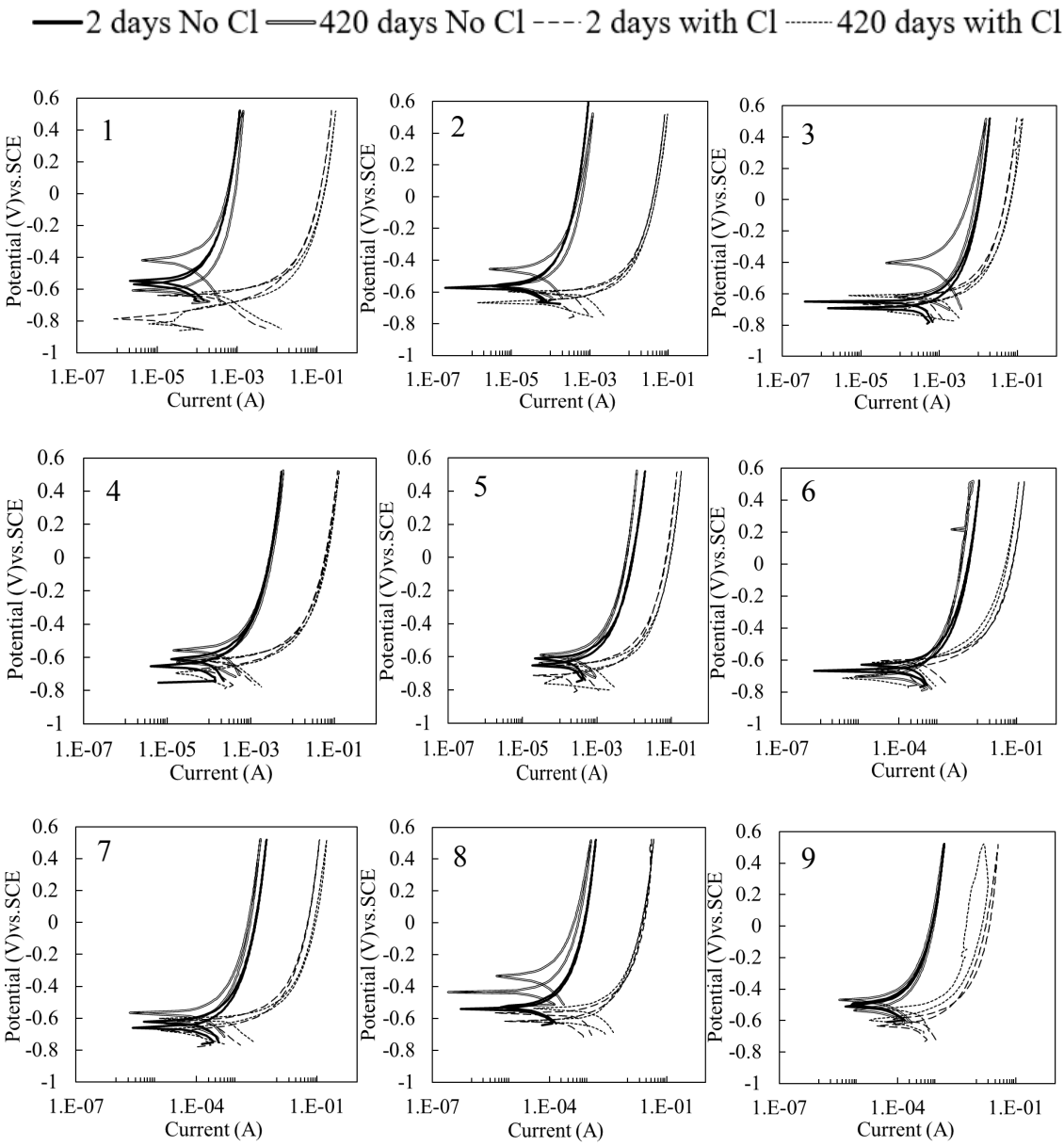

Figure 3. 13. Cyclic polarization plots for one of the steel-mortar specimens in each soil (1 to 9 according to Table 3.2), after 2 days and 420 days exposure to chloride free and 2 days and 400 days exposure to 3% by weight chloride contaminated soils.

The addition of salt caused significant changes in all specimens. For steel specimens, as the time of exposure increased, corrosion activity also increased.

The galvanic current between specimens in the soils with and without the addition of chloride was calculated using the results from the ZRA test and are shown in Figure 3.14. As can be seen, galvanic current existed in all cases and the current flowed from specimens in soils with elevated chloride content to the specimens in the as-received soils. The galvanic current was minimum in soils 3 and 5. Galvanic behavior depends on different factors such as geometry, surface area ratio and mass transport (Oldfield 1988). However, for both specimens in the coupled cell, the galvanic behavior could only be attributed to the difference in the chloride levels in the soil; with the chloride acting as an oxidizing species.

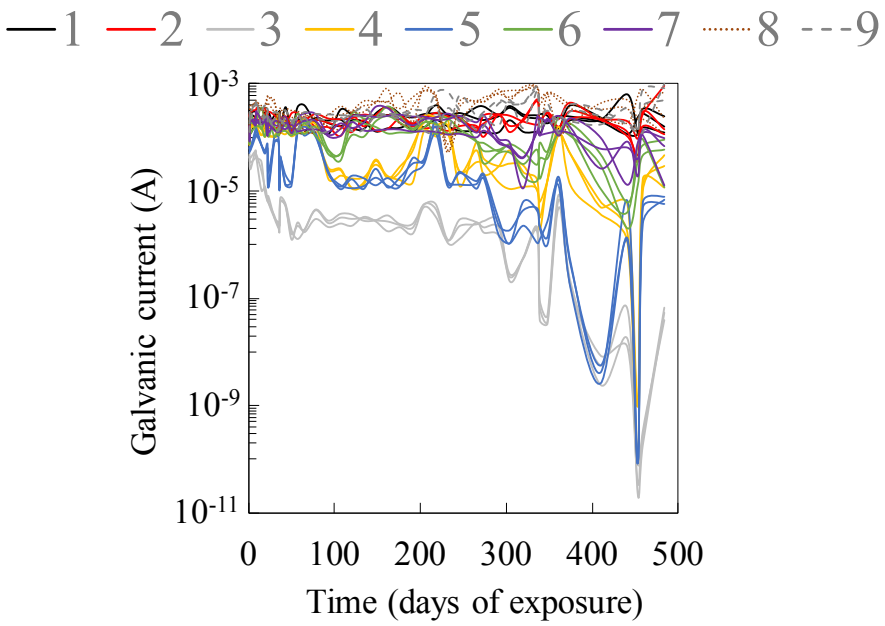

Figure 3. 14. Galvanic current, obtained from the ZRA test on as received specimens in chloride free and 3% by weight chloride contaminated soils.

Figure 3.15 shows the corrosion potential and the corrosion current density values of the as-received and sandblasted specimens embedded in soil 9. As can be seen, the sandblasted

specimens showed more positive potential values compared to that for the as-received specimens. The sandblasted specimens also showed considerably lower corrosion activity compared to the as-received specimens. These results corresponded well with the results from corrosion potential measurements.

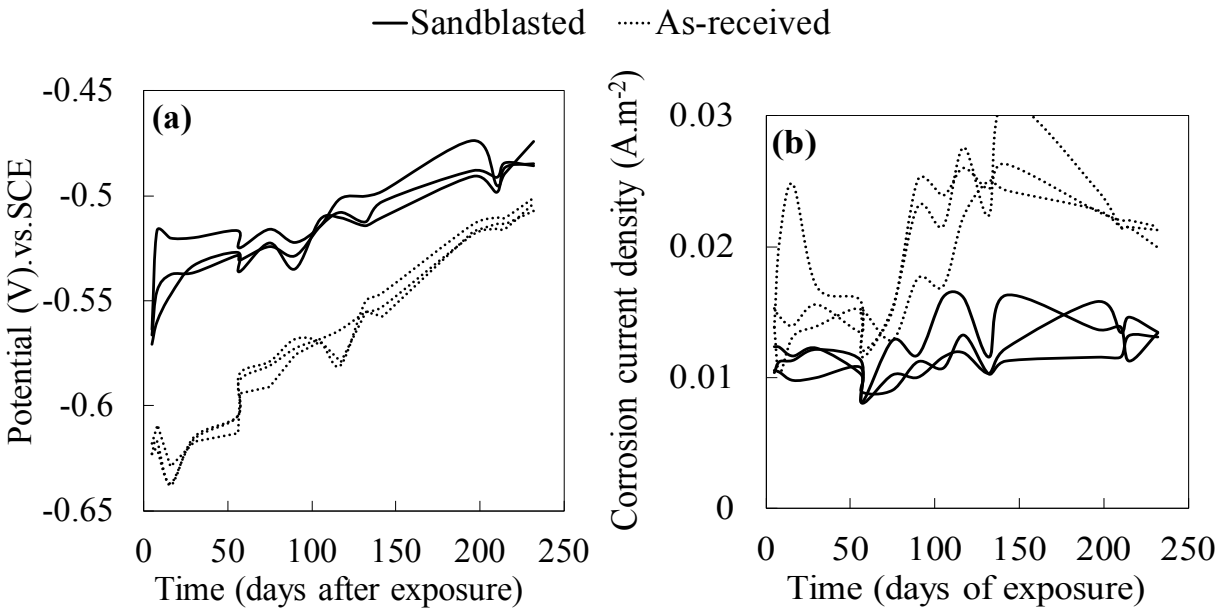

Figure 3. 15. (a) Corrosion potential values and (b) corrosion current densities of the as-received and sandblasted specimens in soil 9.

The mass loss in each specimen can be calculated by determining the area under each curve in Figure 3.15(b) and using Faraday's law (Poursaee 2011). Figure 3.16 shows the calculated mass loss of the specimens. The mass loss of the as-received specimens was approximately 70.5% higher than that for the sandblasted specimens. It should be noted that this observation might be valid only for the exposure condition used in this

investigation. These results clearly showed that when the surface of the steel was sandblasted, the corrosion rate decreased significantly.

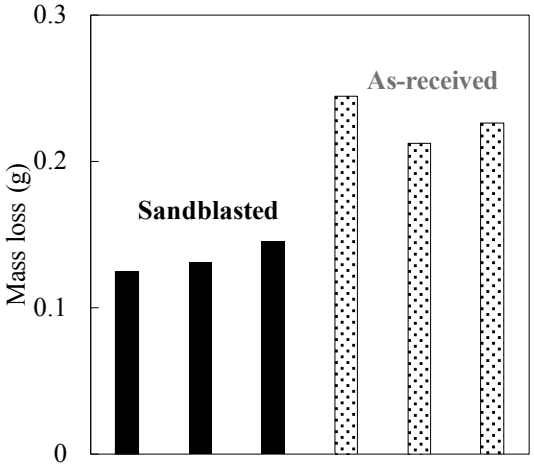

Figure 3. 16. The calculated mass loss for sandblasted and as-received steel specimens during 232 days of being embedded in the soil.

Figure 3.17 shows the corrosion potential values and corrosion current densities of both new (as-received) and old rusted steel in water; the vertical dash line represents the date of chloride addition. As can be seen, after the addition of chloride, new steel showed more negative corrosion potential compared to the old rusted specimens. The old rusted specimens showed higher corrosion current densities compared to the as-received specimens since the first day of the addition of chlorides.

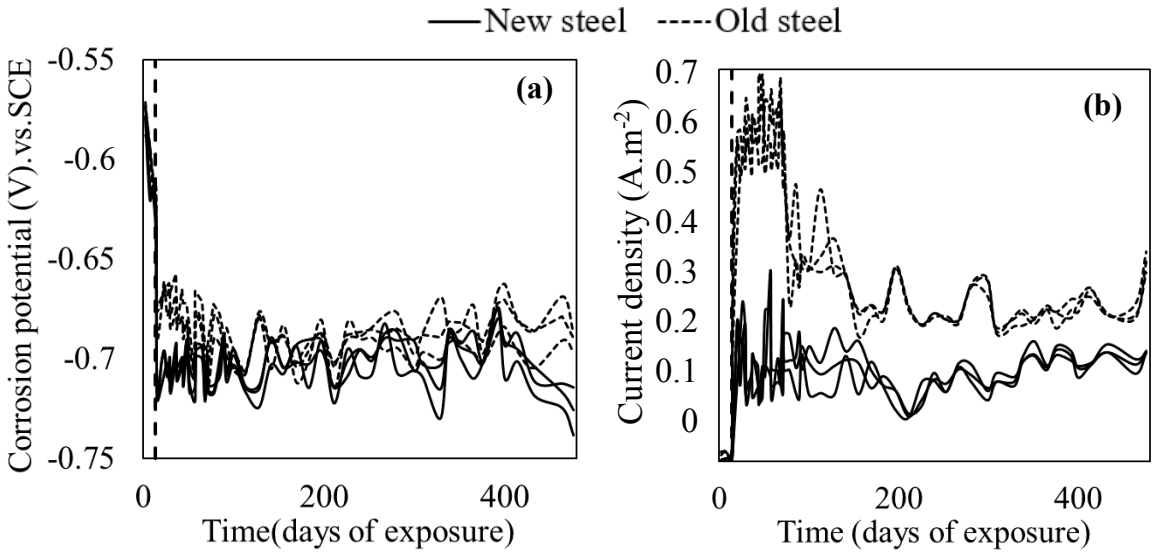

Figure 3. 17. (a) Corrosion potential values and (b) corrosion current densities of new and old steels in water. Vertical dash line represents the data of chloride addition.

Figure 3.18 shows the galvanic corrosion current of coupled old and new steel in chloride free and 3% by weight chloride contaminated tap water. As can be seen, galvanic current existed in all case and the current flowed from specimens in water both with and without chlorides. Coupled specimens exposed to the chloride-contaminated water showed higher galvanic current compared to those in the chloride-free water. The direction of the current was from old to new specimens, indicating enhancing the increase in corrosion on the old specimens.

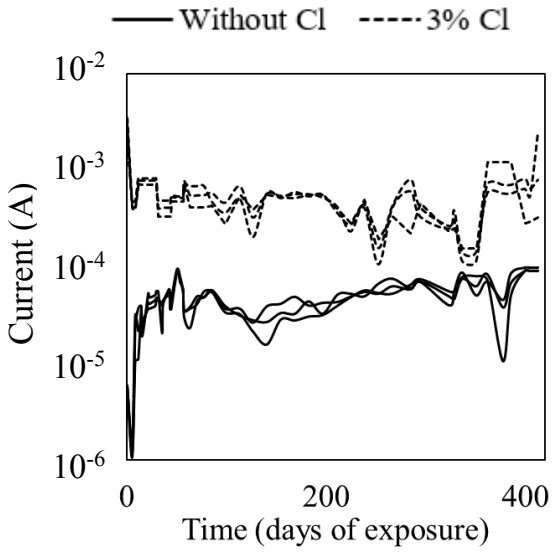

Figure 3. 18. Galvanic current, obtained from the ZRA test on new and old steel in chloride-free and 3% chloride contaminated tap water.

3.6. Summary

This chapter aimed to study the corrosion performance of carbon steel in different soils, collected from the state of Wisconsin. Carbon steel specimens (as-received) as well as steel embed in mortar (steel-mortar) specimens, to simulate the realistic H-pile design in bridges, were used in this investigation. Both as-received steel and steel-mortar specimens were embedded in as-received soils, with different physiochemical properties, i.e. pH, moisture content, resistivity, chloride content, sulfate and sulfite contents, and the mean total organic carbon concentration, for more than one year. Both specimen types were also embedded in the same as-received soils, but with increased chloride content to 3% by weight of chloride ions for more than one year. In addition, the surface of three identical as-received specimens was modified using the sandblasting method for 5 minutes. These

specimens were embedded in one of the collected soils. Different electrochemical measurements were conducted on the specimens to evaluate the corrosion activity of the steel in these soils. The results showed a decrease in corrosion activity of the steel-mortar specimens in all soils compared to the as-received specimens in the same soil both with and without chlorides. Both steel and steel-mortar specimens showed higher corrosion activity in the soils with high sulfate contents compared to the other soils. In all cases, there was a galvanic current flowing between specimens in chloride-free and chloride contaminated soils. In addition, corrosion potential values of all specimens remained relatively stable both before and after addition of chlorides, suggesting just measuring the corrosion potential may not be an efficient method to monitor the change of corrosion behavior of steel in the soil. The results of electrochemical experiments also showed significant improvement in corrosion resistance of sandblasted specimens compared to the as-received specimens. In summary, it is found that:

1. In general, (except soil 8) the steel-mortar specimens and as-received specimens showed comparable corrosion activities in both as-received soils and soils with elevated chloride content.
2. As-received steel specimens in as-received soil 3 showed the highest corrosion current densities less than 0.6 $A.m^{-2}$ compared to other as-received specimens.
3. When chlorides were added, the steel-mortar specimens in soils 8 and 9 showed higher corrosion current densities compared to the other specimens.
4. Corrosion potential values of all specimens remained relatively stable, both before and after the addition of chlorides, while the corrosion current densities increased

after addition of the chlorides. Thus, based on this result, measuring just the corrosion potential was not an efficient and accurate method to evaluate the corrosion behavior of the steel in the soil.

5. After measuring the actual corroded areas on each specimen, the results of the current density measurements were significantly changed.
6. The physiochemical parameters available for the soils could not be used to explain the observed behaviors. It was hypothesized that the synergistic activity of the chlorides and SRB was the reason for a significant increase in the corrosion rates of steel in soil 9. However, no information was available on the type and population of the bacteria in the soils to support this hypothesis.
7. The galvanic corrosion was also observed between steel in soils with the same chemistry but different chloride contents.
8. Sandblasting significantly enhanced the corrosion resistance of the steel in soil compared to as-received specimens. The mass loss of the as-received specimens was approximately 70.5% higher than that for the sandblasted specimens.
9. Old steel specimens retrieved from the bridge showed higher corrosion activity (0.3 $A.m^{-2}$) compared to the new as-received steel (0.1 $A.m^{-2}$). This point needs to be considered during repair and maintenance if such combination is expected.

CHAPTER 4

4. APPLICATION OF THE GENERALIZED REGRESSION NEURAL NETWORK METHOD FOR CORROSION MODELING OF STEEL EMBEDDED IN SOIL*[1]

4.1. Introduction

Several modeling approaches and methodologies were used for the prediction of corrosion of steel in different scenarios such as the multiple regression technique (Haynie and Upham 1974, Feliu and Morcillo 1993, Hou 1993, Morcillo, Simancas et al. 1995), support vector regression (Vapnik 1995, Smola and Schölkopf 2004, Wen, Cai et al. 2009); the fuzzy-set-based technique (Jang 1993, Kartalopoulos and Kartakapoulos 1997, Smola and Schölkopf 2004, Novák, Perfilieva et al. 2012, Mousavifard, Attar et al. 2015); and neural network modeling (Cai, Cottis et al. 1999, Pintos, Queipo et al. 2000, Morcous and Lounis 2005, Parthiban, Ravi et al. 2005). Some of the above-mentioned models (i.e. multiple regression technique) have been shown to be effective only in very restrictive environments and are limited to capture the corrosion activity with limited variables. In addition, none of these studies has been applied to study the corrosion of steel in the soil environment. Among these methods, neural network methodology seems cable of modeling the corrosion process of steel in such an environment.

[1] *A similar form of this chapter has been submitted at the time of writing: Ding, L, Poursaee, A. Application of the generalized regression neural network method for corrosion modeling of steel embedded in soil.

Neural networks are computational systems whose architecture and operation are inspired by people's knowledge about biological neural cells (neurons) in the human brain (Gupta and Gupta 1979, Hertz, Krogh et al. 1991, Shahin, Jaksa et al. 2001, Neaupane and Achet 2004, Lin, Chang et al. 2009, Pradhan and Lee 2010). Neural networks have been used as promising tools in corrosion research (Helliwell, Turega et al. 1996, Cottis, Qing et al. 1999, Pintos, Queipo et al. 2000, Parthiban, Ravi et al. 2005, Fang, Wang et al. 2008). These systems are suitable for the approximation of relations among non-structured data with a high degree of nonlinearity and incomplete data. Neural networks are particularly suitable for modeling the complex systems due to their capability of learning, adapting and generalization from measured data (Jančíková, Roubíček et al. 2008, Jančíková, Zimný et al. 2013).

Rosen and Silverman used the neural network technique on the data from potentiodynamic polarization scan to identify if crevice, pitting and general corrosion are concerns (Rosen and Silverman 1992). Trasatti and Mazza successfully predicted the crevice corrosion of stainless steel and related alloys in a near neutral chloride contaminated environment using a neural network (Trasatti and Mazza 1996). This technique was also used to describe the risk of stress corrosion cracking (SCC) as a function of temperature, chloride concentration and oxygen content (Smets and Bogaerts 1992).

Establishing a predictive model from the measured corrosion data collected from soil can be hardly solved by classic methods of statistic data evaluation (e.g. regression analysis).

Nevertheless, as far as the authors are concerned no study was carried out to model corrosion of steel in a soil environment using a neural network. This paper presents the development of a Generalized Regression Neural Network (GRNN) based model for the modeling and prediction of the corrosion current densities and corrosion potential of carbon steel embedded in the limited number of soils with different physicochemical parameters, including pH, moisture content, resistivity, chloride, sulfate, sulfite, and mean total organic carbon concentrations in soils. There are other factors that can potentially lead to the corrosion of steel in soil environments (e.g. oxygen level), which are not considered in this study. It should be emphasized that this study was focused on the initiation and development of a preliminary neural network-based model and the data used to develop the model were obtained from nine soil samples. Authors are currently working on using data from the National Bureau of Standards (NBS) to improve their model and the result will be submitted for publication in the near future.

4.2. Generalized Regression Neural Network (GRNN)

System identification is a methodology used for building mathematical models of dynamic systems from measurements of the system inputs and outputs (Graupe 1972). The applications of system identification include any system where the inputs and outputs can be measured. This includes industrial processes, control systems, economic data, biology, and the life sciences, medicine, social systems and many more (Natke 2014). Specht proposed a generalized regression neural network (GRNN), a procedure that used neural

networks for identification and control of nonlinear systems and involved one-pass learning (Specht 1991). GRNN is basically a neural network-based function approximation or function estimation algorithm which predicts the output of given input data. Any neural network method principally needs training data, which contain input-output, to train itself. By training the network with the training data set, the network can then predict the output/results of feeding new test data set. GRNN falls into the category of probabilistic neural networks. The use of a probabilistic neural network is especially advantageous because the network "learns" in one pass through the data and can generalize from examples as soon as they are stored (Specht 1991). In other word, the network is capable to converge to the underlying function of the data with only a few training samples available. In the GRNN approach, the regression of a dependent variable y on an independent x estimates the most probable value for y, if a training set is available. The regression method produces the estimated value of y which minimizes the mean-squared error.

The data available from measurements of an operating system is generally never enough for a backpropagation neural network (Specht 1991). Therefore, the use of GRNN is especially advantageous due to its ability to predict results with only a few training samples available and the additional knowledge needed to get the fit in a satisfying way is relatively small.

4.3. Algorithm

In GRNN, the weighted average of the outputs of training dataset is used to estimate the output. The weight is calculated using the Euclidean distance between the training data and test data (Specht 1991). The probability density function used in GRNN is the normal distribution and stands on the following equation:

$$\hat{Y}(X) = \frac{\sum_{i=1}^{n} Y_i \exp(-\frac{D_i^2}{2\sigma^2})}{\sum_{i=1}^{n} \exp(-\frac{D_i^2}{2\sigma^2})} \tag{4.1}$$

where,

$$D_i^2 = (X - X_i)^T (X - X_i) \tag{4.2}$$

X is the input sample, X_i is the training sample, Y_i is the output of the input sample X_i, D_i^2 is the Euclidean distance from X, $\exp(-\frac{D_i^2}{2\sigma^2})$ is the activation function, and T means the matrix transpose. The contribution of the training sample is determined by the activation function. The Euclidean distance between the training sample and the point of prediction, is used as a measure of how well each training sample can represent the position of the prediction, X. If the Euclidean distance between the training sample and the point of prediction is small, the activation function becomes relatively large value, and if it is a large value, the activation function becomes relatively small value; therefore, the contribution of the remained training samples to the prediction is relatively small. If the Euclidean function is zero, the activation function becomes one and the point of evaluation is represented as the best by this training sample. σ is spread constant. When σ is large, the estimated density is forced to become smooth and it becomes a multivariate Gaussian.

On the other hand, a smaller value of σ allows the estimated density to assume non-Gaussian shapes (Specht 1991). Spread constant should be adjusted by the training process to minimize the error.

The objective of the training procedure is to determine the optimum value of the spread constant (σ). The best approach is finding where the mean square error (MSE) is minimum. MSE measures the performance of the network according to the equation 4.3:

$$MSE = \frac{1}{n}\sum_{i=1}^{i=n}[(Y_{GRNN})_i - (Y_{exp})_i]^2 \quad (4.3)$$

where n is the number of data points, $(Y_{GRNN})_i$ is the GRNN prediction and $(Y_{exp})_i$ is the experimentally measured data. For this purpose, the input data should be divided into two sets of data: (i) training dataset and (ii) testing dataset. Then, the GRNN should be applied on the second set (testing) based on the first set (training) and the MSE for different spread constants should be calculated. The corresponding value of σ to the minimum MSE should be determined and used in the rest of the modeling steps.

To evaluate the test results, the multiple correlation coefficient, R^2, and the mean absolute percentage error, MAPE, can be used:

$$R^2 = \frac{\sum_{i=1}^{n}(\hat{y}_i - \bar{y})^2}{\sum_{i=1}^{n}(y_i - \bar{y})^2} \quad (4.4)$$

$$\text{MAPE} = \frac{1}{n}\sum_{i=1}^{n}\left|\frac{\hat{y}_i - y_i}{y_i}\right| \quad (4.5)$$

where n denotes the number of test samples, y_i represents the i^{th} experimentally measured value, $\hat{y}_i$ is the predicted value for the i^{th} test data, and $\bar{y}$ is the mean measured value for all test data.

4.3.1. Construction of the GRNN

The MATLAB codes were written for the generalized regression algorithm. GRNNs consisted of two steps. The first step was the training of the neural network. The physicochemical variables of soil samples, as well as the exposure time of specimens in soils, were used as input, corresponding to X in the equation 4.1, and the experimental data from measurements of corrosion current densities and corrosion potentials of the steel specimens were used as training input, corresponding to Y_i in equation 4.1. The simulated corrosion current densities or corrosion potentials were the outputs of the network as shown in layer four in Figure 4.1. Since the input parameters were in different ranges, these parameters were normalized within 0.1-1 ranges to prevent the simulated Euclidean distance from being driven too far. The data from 5 months of measurements were used for building the model. Table 4.1 lists the statistical information on the corrosion and variables data used in this work. The corrosion current densities and corrosion potential values measured from three identical specimens (Figures 4.2a and 4.2b) were combined. 70% of these data were selected randomly and used for training (number of data sets=2930), the same data were used for validation (number of data sets=2930), and the rest 30% were used for testing (number of data sets=1256). In this model, the network structure with spread constant σ=1 provided the best performance, i.e. minimum MSE.

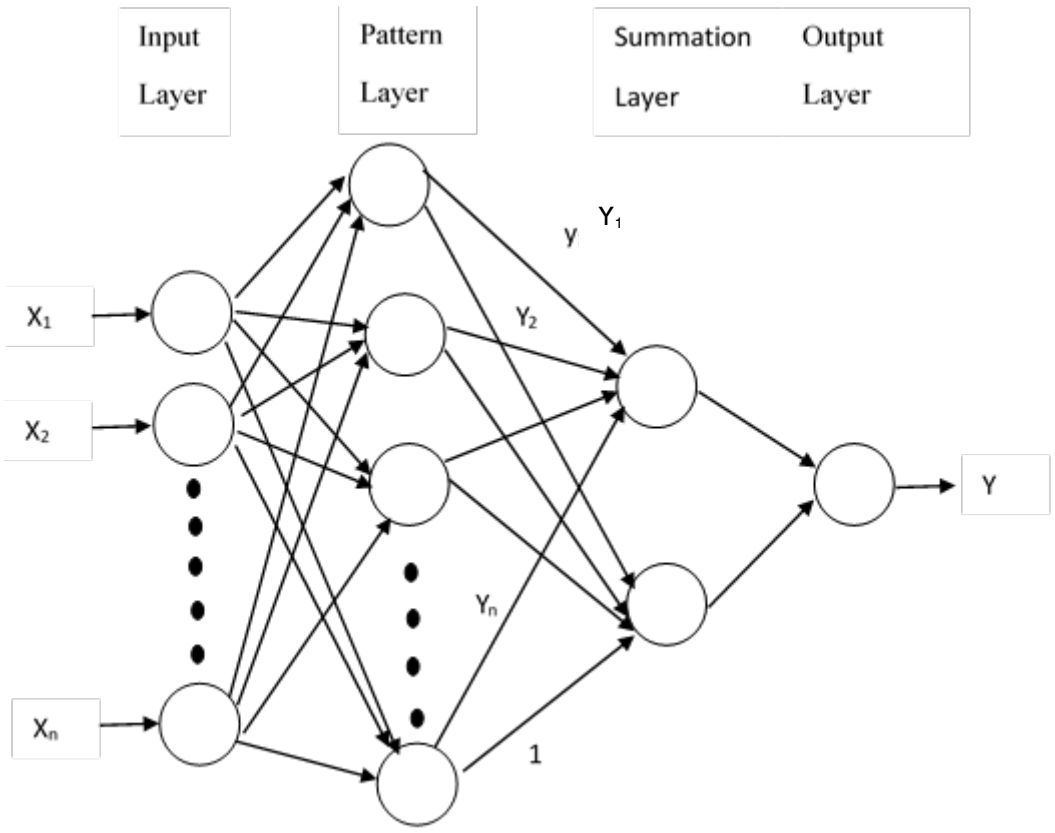

Figure 4. 1. Schematic diagram of GRNN architecture.

After a number of trials, the best network architecture and parameters that minimize the MSE error of training data were selected as follows:

- 8 input units;
- 2 hidden layers;
- 8 hidden units;
- 1 output unit;
- Activation function= Gaussian function;
- learning rate=0.1;

- learning cycles=1000

Table 4. 1. Fundamental statistical information associated with the data set used for the construction of the GRNN model.

Variables	Minimum	Maximum	Mean	S.D.	Range
Moisture content (%)	8.8	66.9	31.41	18.70	58.1
pH	6.08	7.9	7.16	0.55	1.82
Resistivity (<OMEGA>-m)	1000	66800	19922.22	21910.56	65800
Chloride (wt%)	0.006	0.727	0.19	0.25	0.721
Sulfate (mg/kg)	24.7	219.0	64.84	64.95	194.3
Sulfide (mg/L)	20	54.7	23.85	10.90	34.7
MTOC* (mg/kg)	614	262000	42493.44	78642.42	261386
Exposure time (days)	0	155	77.5	45.03	155
Corrosion potential (V)	-0.935	-0.265	-0.67	0.10	0.67
Corrosion current densities ($A.m^{-2}$)	0.0105	0.4690	0.1536	0.0594	0.4585

4.4. Results and discussion

4.4.1. Experimental results

Table 4.2 shows the average Tafel slopes and the calculated Stern-Geary constants of the specimens in different soils.

Table 4. 2. Tafel slopes (βa and βc) and calculated Stern and Geary Constants (B).

Soil sample ID	βa	βc	B
1	0.53	0.21	0.03
2	0.31	0.44	0.04
3	0.57	0.51	0.13
4	0.33	050	0.06
5	0.49	0.36	0.06
6	0.38	0.43	0.05
7	0.43	0.34	0.05
8	0.23	0.40	0.02
9	0.38	0.31	0.03

Figures 4.2a and 4.2b show the corrosion current densities and corrosion potential values of the specimens measured for 5 months, respectively.

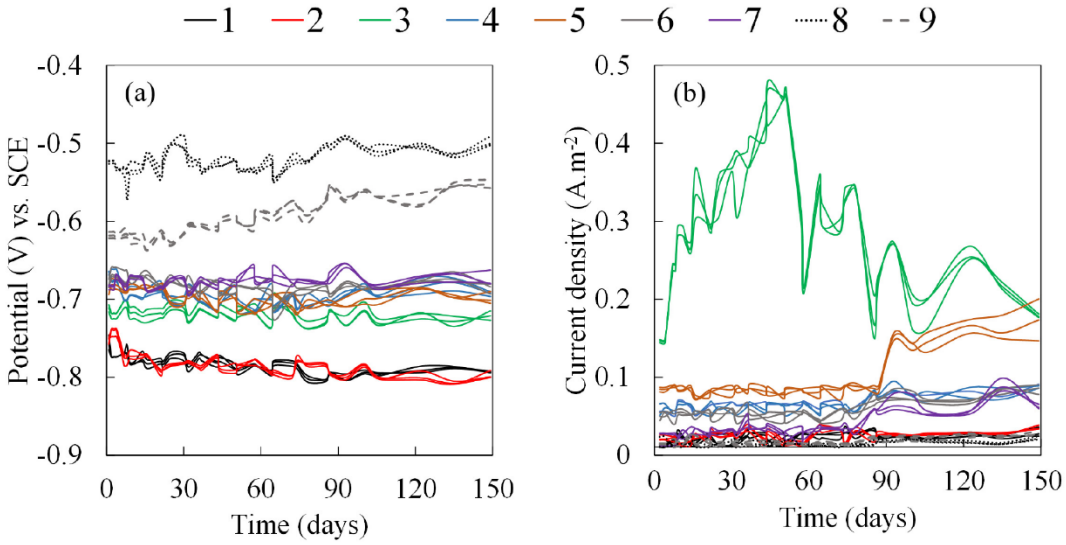

Figure 4. 2. (a) Corrosion potential values and (b) corrosion current densities of all specimens in 9 different soils with specifications given in Table 3.2.

4.4.2. Training and testing of the original data

Table 4.3 shows the correlation coefficient (R^2), MSE and MAPE obtained from the GRNN model.

Table 4. 3. R^2, MSE, and MAPE calculated using the information obtained from the GRNN model.

	Correlation coefficient (R^2)	**MSE**	**MAPE (%)**
HCP training set	0.9995	0.0005159	0.4031
Corrosion current density training set	0.9983	0.001645	1.420
HCP validation set	0.9936	0.0008545	0.4471
Corrosion current density validation set	0.9633	0.03127	12.948
HCP Testing set	0.9990	0.006920	1.165
Corrosion current density testing set	0.9979	0.001879	1.565

As can be seen, statistically, the GRNN model could account for more than 96% of the variance of the corrosion current densities and corrosion potential values of the steel specimens embedded in different soils. It can also be noted that the MSE and MAPE indexes of corrosion potential values estimated by GRNN models were both less than those of corrosion current densities for training, validation, and testing; indicating that the prediction accuracy of corrosion potential values was greater than those of corrosion current densities. The results of R^2 corresponds well with MSE and MAPE, which reveals that the regression effect fitted by corrosion potential values was better than that of corrosion current densities.

The significance of an input on determining of output can be evaluated by some various methods. Utilizing the fuzzy curve is one of these methods which had been proved to be better than the other (Sung 1998). The concept of the fuzzy curve is developed by Lin and Cunningham (Lin and Cunningham 1995) and has been addressed previously in several corrosion studies (Sturrock and Bogaerts 1997, Javaherdashti 2000, Singh and Markeset 2009). This concept is intended to be used on a multi-input, single output system, so it was utilized in this work. In order to determine the effect of each parameter on the corrosion current density, a fuzzy curve was performed, and it is shown in Fig.4.3.

Figure 4.3 shows the fuzzy curves for the parameters in Table 3.2. The significance of a variable is measured based on the range the fuzzy curve spans on the C-axis, which is mentioned in the legend of Figure 4.3. If the fuzzy curve for a given input is flat, then this input has little influence in the output data and it is not a significant input. We ranked the importance of the input variables according to the range covered by their fuzzy curves *Ci*. The range of fuzzy curves in Figure 4.3 are 0.23 for moisture, 0.3 for pH, 0.55 for resistivity, 0.9 for chloride, 0.96 for sulfate, 0.35 for sulfide and 0.4 for MTOC. As revealed by results in Fig.4.3, the sulfate and chloride levels are the two most significant variables followed by the resistivity, respectively. Also, the fuzzy curve indicates that the influence of moisture content, pH, sulfide level and mean total organic carbon are less important than the other factors within the studied range.

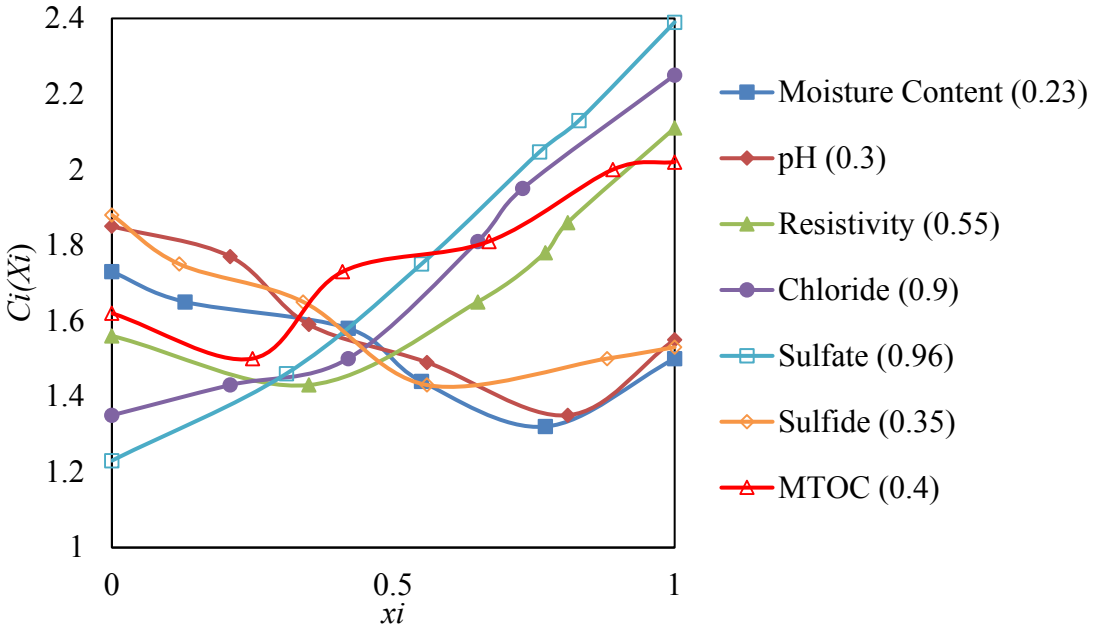

Figure 4. 3. Fuzzy curves for input factors. The range of each fuzzy curve is indicated in the legend.

4.4.3. Sensitivity analysis

Sensitivity analysis explores the sensitivity of a model's outputs to changes in parameter values (Railsback and Grimm 2011). Sensitivity analysis is imperative for understanding the relationship between input parameters and outputs, testing the robustness of the output, and identifying errors in the model. Comparing the weights between nodes of the input layer and nodes of the hidden layer, showed that the magnitude of the weight of moisture and chloride contents were larger than the other parameters. Thus, the sensitivity analysis conducted on the trained neural network to study the effects of moisture and chloride contents on the corrosion current densities and corrosion potential values. As can be seen in Figures 4.4 and 4.5, a positive linear relationship between both chloride and moisture

contents and corrosion current densities; and a negative linear relationship between both chloride and moisture contents and corrosion potential values, indicated significant impact of these variables on the corrosion current densities and corrosion potential values of steel specimens in different soils.

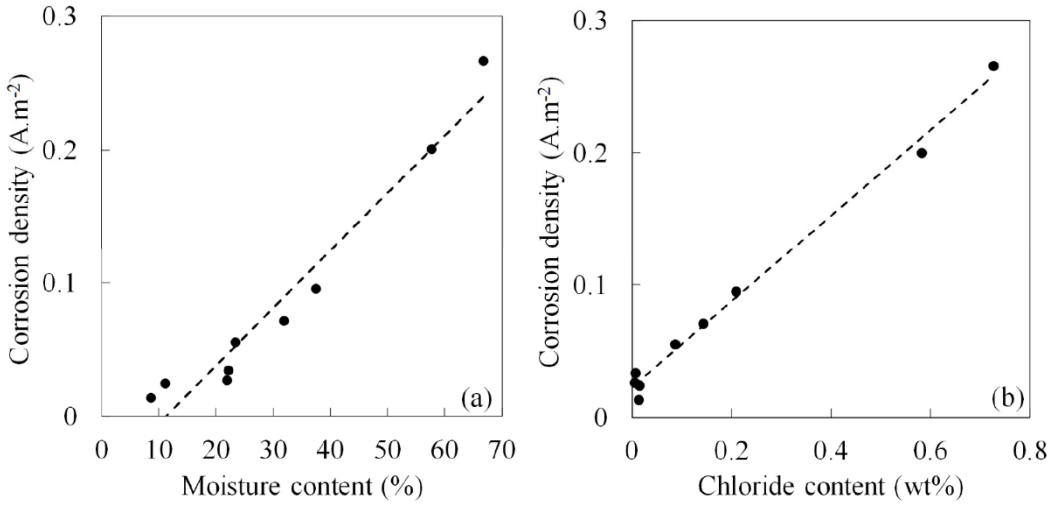

Figure 4. 4. Effect of (a) moisture content and (b) chloride content of soil on the corrosion current densities.

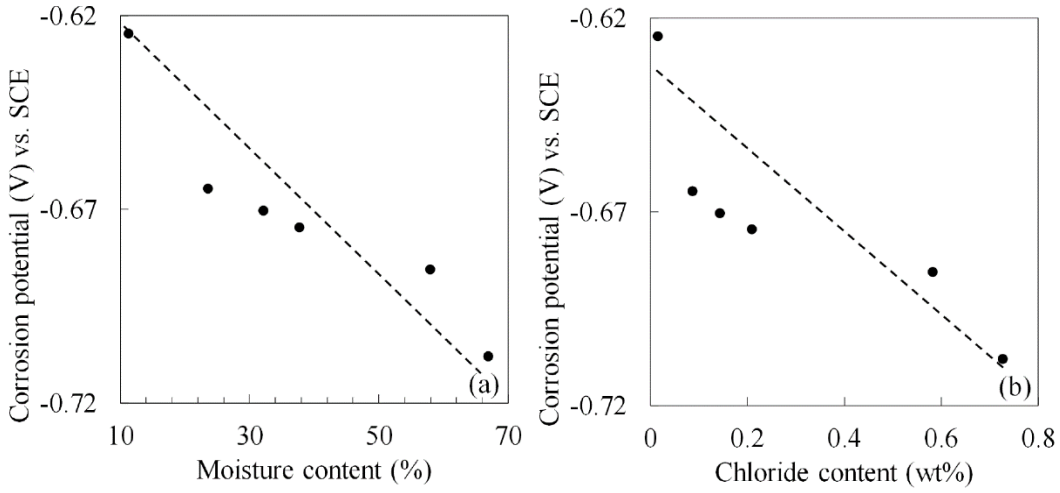

Figure 4. 5. Effect of (a) moisture content and (b) chloride content of soil on corrosion potential values.

4.5. Case studies

4.5.1. Case study I: prediction of corrosion current densities and corrosion potential values of steels by changing chloride concentration of the soil

Based on the results of the sensitivity analysis, shown in Figures 4.4 and 4.5, increasing the chloride content of the soil, significantly increases the corrosion activity of the embedded steel specimens. To experimentally explore the impact of increasing the chloride content on the corrosion activity of the steel specimens and to evaluate the performance of GRNN model on the prediction of corrosion behavior, the chloride content of the soils was increased to 3% by weight and laboratory experiments were conducted on the steel specimens.

Figures 4.6a and 4.6b show the comparison between the predicted and the experimentally measured corrosion current densities and corrosion potential values, respectively. The predicted results were achieved by changing one of the input vectors (chloride content) in the algorithm in the original GRNN model described before.

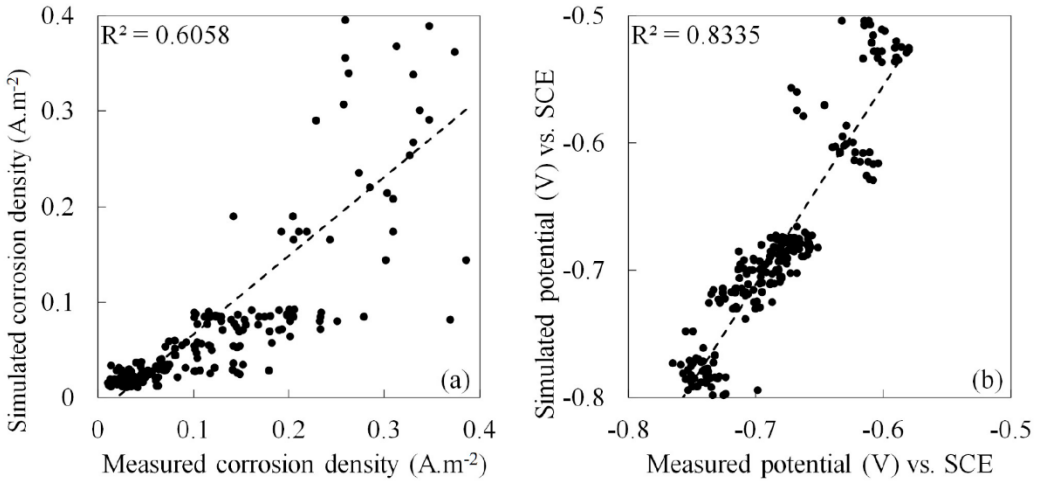

Figure 4. 6. Comparisons of measured and predicted (a) corrosion current densities and (b) corrosion potential values after increasing the chloride concentration of soils to 3% by weight. Original GRNN model was used.

The R^2 values of 0.605 and 0.833 for current densities and corrosion potential values, shown in Figure 4.6, indicated reasonable prediction by the model. However, to enhance the performance of the model, the model has undergone another training process.

The maximum value of the chloride concentration of the as-received soils was 0.727%, which was 2.273% points less than that after increasing chlorides level to 3% by weight. This changing had a significant effect on the Euclidean distance and activation function in the original model. Thus, to improve the model, 50% of the soil parameter data after adding chloride as inputs as well as 50% of the corrosion current densities and corrosion potentials as outputs were combined with original data used for training, and the rest 50% were used for testing. Table 4.4 shows the GRNN performance for the steel specimens after this procedure.

Table 4. 4. GRNN performance for ASTM A572-50 steel after adding chloride.

	Correlation coefficient (R^2)	**MSE**	**MAPE (%)**
HCP training set	0.9997	0.0004368	0.04031
Corrosion current density training set	0.9905	0.03954	12.57
HCP validation set	0.9986	0.001526	1.469
Corrosion current density validation set	0.9934	0.009839	5.623
HCP Testing set	0.9661	0.06375	27.59
Corrosion current density Testing set	0.8816	0.5691	47.63

Clearly, training the model significantly improved its prediction capability. The model was run using the remaining data that were not used in the training and validation steps. The comparison between predicted, obtained from the newly trained model, and the measured data of steel specimens after increasing chloride concentration are shown in Figures 4.7a and 4.7b. As can be seen, after training the model, the results of the prediction were close to the directly measured values from the experiments and good correlation existed among the measured and the predicted values as shown in Table 4.4.

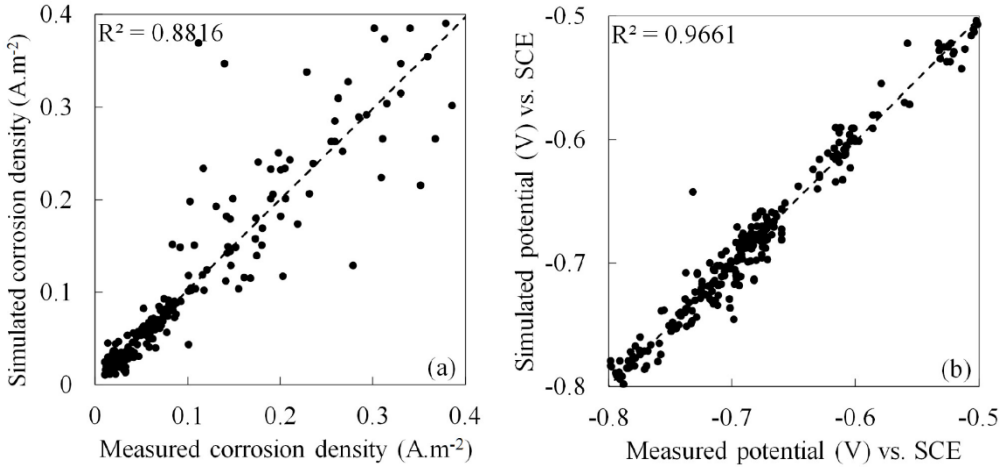

Figure 4. 7. Comparisons of measured and predicted (a) corrosion current densities, and (b) corrosion potential values, after increasing the chloride concentration of soils to 3% by weight. The original GRNN model was trained again.

4.5.2. Case Study II: Prediction of the corrosion current densities and corrosion potential values of steel specimens in different soils ahead of the experimental measurements

To evaluate and validate the performance of the model in the realistic prediction of the corrosion behavior of the embedded steel specimens, the re-trained GRNN model described in Case Study I was used to predict the corrosion current densities and corrosion potential values of steel specimens in all soils 10 weeks ahead of the actual experimental measurements. Then, after the time was reached, the measurements were conducted, and the results were compared with the predicted values. As shown in Figures 4.8a and 4.8b, the predicted values were very close to the measured values and the model can effectively predict the performance of steel specimens.

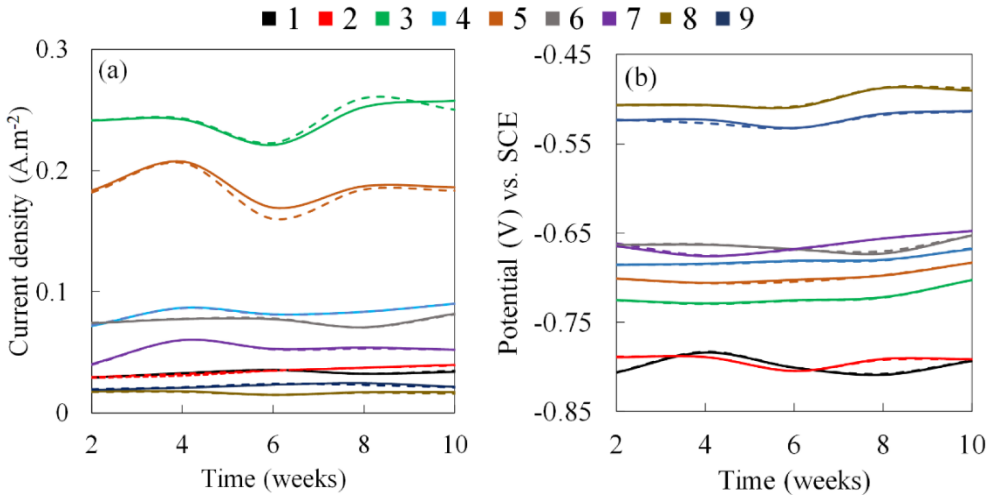

Figure 4. 8. Comparisons of the measured and predicted (a) corrosion current densities and (b) corrosion potential values 10 weeks ahead of actual experimental measurements. Dash lines and solid lines represent the measured and the predicted data, respectively.

4.6. Summary

In this chapter, a generalized regression neural network (GRNN) model used to predict the corrosion potential values and corrosion current densities of ASTM A572-50 steel specimens embedded in nine soils with different physiochemical properties, i.e. pH, moisture content, resistivity, chloride content, sulfate and sulfite contents, and the mean total organic carbon concentration. Experiments were conducted, and the corrosion current densities and corrosion potential values of the steel specimens embedded in different soils were measured. The results obtained from the GRNN model and the experiments exhibited very good agreement, suggesting that the proposed model was capable of predicting the corrosion activity of the steel specimens embedded in different soils.

In summary, it is found that:

1. A very good correlation between the corrosion potential values and corrosion current densities obtained from the GRNN model and the experimental measurements was observed for the as-received soils. The sensitivity analysis was conducted on two input parameters, i.e. chloride content and moisture content. Results showed that changing these parameters had a significant impact on the corrosion current densities and corrosion potential values of the steel specimens. The chloride content of the as-received soils increased and the original model was run. Results showed that while the initial model could predict the corrosion activity of the steel specimens, the accuracy of the prediction was not very high (R^2=0.60). The model was trained again and the performance of the new model in predicting the corrosion activity of the steel in the soils with elevated chloride content was enhanced significantly (R^2>0.88).
2. The model was used to predict the corrosion current densities and corrosion potential values of the steel specimens ahead of the actual experimental measurements and the results showed that the model is highly capable of predicting these values.
3. To develop this model, the data from soils collected from different areas in the state of Wisconsin were used. The authors tried to establish a methodology in predicting corrosion of steel in the soil. Using the extensive body of data available at the NBS will admittedly enhance the model, which is currently under investigation and the results will be reported soon.

CHAPTER 5

5: THE INFLUENCE OF THE SANDBLASTING AS A SURFACE MECHANICAL ATTRITION TREATMENT ON THE ELECTROCHEMICAL BEHAVIOR OF H-PILE STEEL IN DIFFERENT PH SOLUTIONS*[2]

5.1. Introduction

Studies showed that alteration of the surface structure of a metal can change the mechanical properties as well as corrosion behavior of metals (Liu, Wang et al. 2001, Tao, Wang et al. 2002, Balusamy, Kumar et al. 2010, Chen, Li et al. 2013, Fu, Zhan et al. 2015, Liu, Jin et al. 2015). In general, the surface mechanical attrition treatment (SMAT) technique modifies the surface structure of a metal by applying severe plastic deformation through impacting milling balls or hard particles onto the specimen's surface repeatedly (Liu, Lu et al. 2000, Peyre, Scherpereel et al. 2000, Tao, Wang et al. 2002, Dai, Villegas et al. 2004, Lu and Lu 2004, Multigner, Frutos et al. 2009, Azar, Hashemi et al. 2010, Bagherifard, Slawik et al. 2016, Astaraee, Miresmaeili et al. 2017). Sandblasting (Multigner, Frutos et al. 2009, Multigner, Ferreira-Barragáns et al. 2010, Geng, Sun et al. 2015, Rudawska, Danczak et al. 2016), shot peening (Peyre, Scherpereel et al. 2000, Azar, Hashemi et al. 2010, Jayalakshmi, Huilgol et al. 2016, Pour-Ali, Kiani-Rashid et al. 2017, Pour-Ali, Kiani-Rashid et al. 2018) are the typical SMATs which were successfully used.

[2] A similar form of this chapter has been published at the time of writing: Ding, L, Torbati-Sarraf, H, Poursaee, A, (2018). The influence of the sandblasting as a surface mechanical attrition treatment on the electrochemical behavior of carbon steel in different pH solutions. *Surface and Coating Technology*, 352, 112-119.

The SMAT is an effective method of inducing localized plastic deformation that results in grain refinement down to the nanometer scale without changing the chemical composition of the materials (Liu, Lu et al. 2000, Lu and Lu 2004, An, Du et al. 2013, Chen, John et al. 2013, Petan, Ocaña et al. 2016, Yin, Yang et al. 2016, Benafia, Retraint et al. 2018). It was shown that the severe plastic deformation induced by the SMAT significantly influences the corrosion resistance of a variety of metallic materials (Wang, Yu et al. 2006, Mordyuk, Prokopenko et al. 2007, Hamu, Eliezer et al. 2009, Hassani, Raeissi et al. 2009, Lee, Kim et al. 2009, Hou, Peng et al. 2011, Torbati-Sarraf and Poursaee 2018).

Sandblasting, as a SMAT method, was used for different applications such as enhancing the surface strength (Chintapalli, Rodriguez et al. 2014), alteration of the modification of the surface (Chintapalli, Marro et al. 2013), and cleaning the surface of the metal (Raykowski, Hader et al. 2001). While sandblasting cleans the surface and removes the oxide layer from the surface, it also creates a local plastic deformation and grain modification on the surface (Multigner, Frutos et al. 2009, Yuan, Chen et al. 2015), which may lead to a compressive residual stress beneath the surface layer (Geng, Sun et al. 2015). A study by Wang and Li showed the formation of a nano-crystalline layer on the surface of the sandblasted 304 stainless steel (Wang and Li 2002). This layer decreased the corrosion resistance of the sandblasted specimens significantly compared to the as-received specimens in a 3.5% NaCl solution. On the other hand, an investigation by Hou et al. indicated that sandblasting increased the corrosion resistance of carbon steel in an alkaline

environment (Hou, Fu et al. 1997). Ding and Poursaee also reported the significant improvement in corrosion resistance of the sandblasted specimens in an alkaline environment which was proportional to the increase in the sandblasting time. They hypothesized that the formation of calcium-rich layer combined with the enhanced passive layer on the sandblasted specimens were the reasons for the improvement (Ding and Poursaee 2017).

While there are some studies on the impact of sandblasting on the corrosion resistance of carbon steel, nonetheless, to the best of the author's knowledge, there is no in-depth study on the impact of time of sandblasting on long-term corrosion of carbon steel in the different pH solutions, which was the objective of this work. In this study, the surfaces of the steel sheets were treated by sandblasting for 5, 10 and 15 min and the impact of these treatments on the corrosion activity of carbon steel in acidic, neutral and basic solutions was studied. In addition, Scanning Electrochemical Microscopy (SECM) along with microscopic analysis and micro-hardness measurements were exploited to determine the depth of the affected area as well as the impact of the duration of the sandblasting on the activity of the surface and depth of the affected area.

5.2. Materials and experimental procedures

5.2.1. Steel specimens

Similar steel that was used in previous experiments to study its corrosion at different soil sample from Wisconsin, used here as well.

Specimens with a length of 90mm and a width of 25.4mm were cut and their surfaces were sandblasted by particles with an approximately 750 μm diameter under 350 kPa of air pressure. During sandblasting, the angle between the gun and the specimen was kept approximately 90°. As-received steel specimens (AR), as well as three sets of sandblasted specimens, were used in this study. The as-received specimens were cut from degreased and cleaned as-rolled steel. Specimens were sandblasted for 5 min (SB5), 10 min (SB10), and 15 min (SB15). A wire was welded to one end of each specimen for the electrical connection required for the electrochemical tests. To prevent extraneous and edge effects, all the edge and wired was area was coated with epoxy, as shown in Fig.5.1. Epoxy coating provided a 70×20mm exposure area. The as-received specimens washed and cleaned with ethyl alcohol to remove any possible grease and contaminations and dried immediately with air.

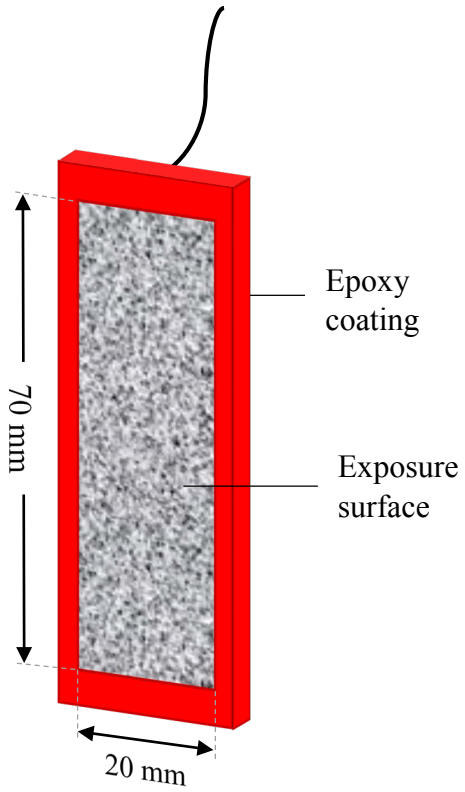

Figure 5. 1. An epoxy coated steel specimen.

5.2.2. Experimental procedures

Optical microscopy was used to investigate the surface microstructure alteration due to sandblasting. In addition, to study the activity and the thickness of the affected area by the sandblasting, cross sections of the specimens were mounted in two-parted cold epoxy. Then, the surface was abraded successively with sandpapers and polished with 1 µm alumina powder. The surface of each mounted specimen was etched in 4% Nital solution for 5 s to reveal its microstructure.

The hardness of the affected area (from the surface toward the center of each specimen) was measured using a Buehler Vickers microhardness tester with a load of 10 g and dwell time of 15 s. Each point corresponded to the average of at least five indentation measurements.

The acidic solution was made of 0.003M HCl with a pH of 2.5. For the neutral solution, the pH of the deionized water was adjusted to 7.1, using 0.1M Na_3PO_4 solution. An aqueous solution with 0.01M NaOH and 0.01M KOH was used to prepare the alkaline solution with a pH of 12.4.

To ascertain reproducibility and reliability of corrosion data, for each set of solution and treatment, a container with three identical steel specimens was prepared. The specimens were immersed in solutions and containers were sealed to minimize atmospheric effects, (e.g. carbonation and change in pH) and possible evaporation. Specimens were immersed in chloride-free solutions for 14 days, then the solution in each measurement cell was partially replaced with 3.5% chloride contaminated solution, and the pH of all solutions was measured and adjusted every day to make sure that the pH stayed constant during the test. Electrochemical measurements were started 24 h after immersing the specimens in the solution and continued for 70 days. All tests were conducted at the laboratory temperature, i.e. ~23 °C.

A three-electrode measurement cell was used for all electrochemical tests. A steel specimen was used as the working electrode and a saturated calomel electrode (SCE) and a 316-stainless-steel sheet were used as the reference and the counter electrodes, respectively. The corrosion potential of the specimens was measured daily. The susceptibility of the specimens to pitting corrosion was evaluated by the Cyclic Polarization (CP) test. For all CP tests, the potential scanned from −50 mV versus open circuit potential to +500 mV versus the reference electrode and reversed to −100 mV versus the reference electrode with the scan rate of 0.1 mV/s. To determine the corrosion current density of the specimens, the Potentiostatic Linear Polarization Resistance (PLPR) technique was used by applying a constant potential of±10 mV versus the corrosion potential to the specimen under test and measuring the resultant current (Ding and Poursaee 2017). PLPR was conducted every three days on each sample. To calculate the polarization resistance (Rp), the Tafel constants (βa and βc), were extracted from the results of the CP tests and used to calculate the value of the Stern-Geary constant. Electrochemical Impedance Spectroscopy (EIS) was also carried out on the specimens. A 10-mV alternating sinusoidal potential perturbation over the frequency range from 10^6 Hz to 10^{-2} Hz was used for the EIS tests. Impedance parameters consisting of a constant phase element (C_{dl}), n, and Rct were extracted from Nyquist plots.

For the SECM, the mounted specimen was placed horizontally, facing upward, in the cell. Scanning probe was a 10 μm diameter platinum microelectrode (UME) inside a capillary

glass (RG[3]~15). Ag/AgCl (saturated KCl) and platinized platinum electrode were used as a reference and counter electrodes, respectively. The surface generated/ tip collection (SG/TC) mode was used in this experiment. Tests were conducted in a buffer solution with the pH=7, with a chemical composition of 8 g/L NaCl, 0.2 g/L KCl, 1.44 g/L Na_2HPO_4, 0.24 g/L KH_2PO_4, and 0.1mM $K_3Fe(CN)_6$ as a redox mediator. The buffer solution was used to assure that the pH level stayed constant within the diffusion layer of the cut edge because of local reactions at the substrate (Tao, Wang et al. 2002, Marques, Izquierdo et al. 2015). The UME was biased at +0.9 V vs. Ag/AgCl for oxidation of mediator. After 5 min immersion in the solution, 300 μm across the polished cross-section of each specimen (from the surface toward the center of the specimen) was scanned with the velocity of 1 μm/s and the generated current from the oxidation of mediator on the tip was recorded.

5.3. Results and Discussion

Figs. 5.2 and 5.3 show images of the morphology, as well as the cross-section of each treated specimen, respectively. As can be seen, relatively similar morphology was obtained during 5- and 10-min sandblasting. However, 15 min sandblasted specimens showed less globular morphology compared to the other sandblasted times. In the cross sections images (Fig. 5.3), severe plastic deformation and flow of material were observed on the surface

[3] $RG=r_{glass}/r_T$, where r_{glass} is the total radius of the probe including glass sheath and r_T is the radius of the Pt electrode.

and subsurface area. The thickness of the affected area was a function of the sandblasting time.

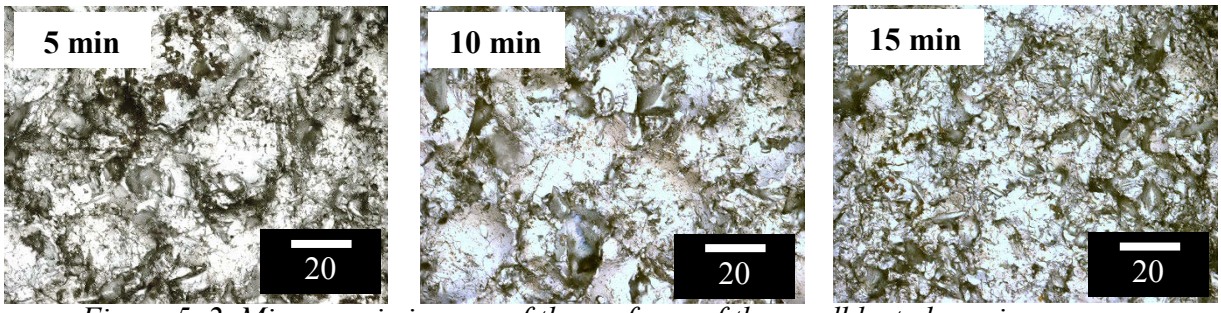

Figure 5. 2. Microscopic images of the surfaces of the sandblasted specimens.

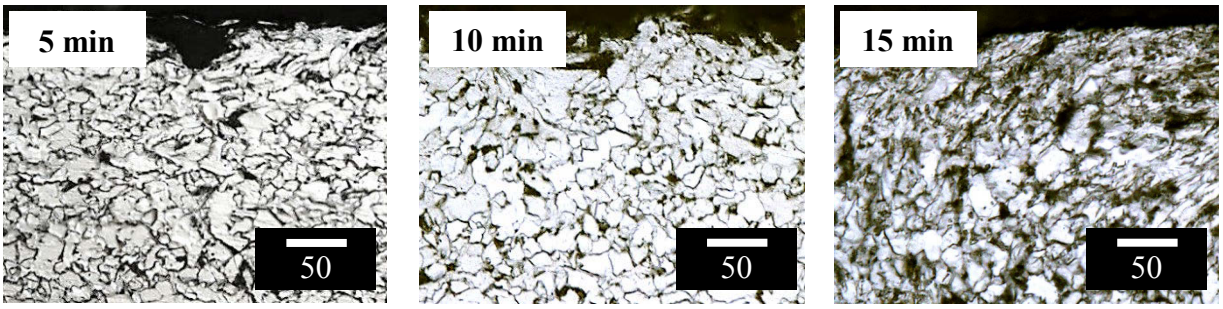

Figure 5. 3. Microscopic images of the cross-section of the sandblasted specimens.

In sandblasting, repeated shock load with high-speed strain rate was applied to the surface, which may cause formation of high-density dislocations (Liu, Wang et al. 2001, Li, Hou et al. 2017), deformation of grains, dissolution of cementite into other grains and ferrite (Balusamy, Kumar et al. 2010), and presumably phase transformation due to high temperature generated during the local intense deformation (Sun, Shi et al. 2008, Chintapalli, Rodriguez et al. 2014, Amanov and Pyun 2017).

Results of the arithmetical mean roughness value, Ra[4], greatest height of the roughness profile, Rz[5], and estimated thickness of the deformed area for the sandblasted specimens are given in Table 5.1. While the thickness of the impacted area was increased by increasing the time of sandblasting, the Ra value increased from 5 to 10 min of sandblasting and stayed relatively constant thereafter.

Table 5. 1. The measured mean grain size of the bulk, roughness, and thickness of the affected area.

Sample	The average grain size of the bulk	R_a (μm)	R_z (μm)	Deformed Thickness (μm)
AR	14±8	0.7±0.3	0.8	-
SB5	14±8	12.7±4.1	16.1	17±7
SB10	14±8	8.9±3.9	12.2	24±9
SB15	14±8	8.1±3.1	8.4	45±10

However, Rz values slightly decreased by increasing the duration of sandblasting, meaning that the height of the peaks and valleys declined by increasing the time of sandblasting, which could be attributed to the increase of the repeated multidirectional impact of the sand particles onto the surface due to their random flying directions from moving gun (Balusamy, Kumar et al. 2010, Chen, Li et al. 2013, Fu, Zhan et al. 2015).

[4] Ra is calculated by an algorithm that measures the average length between the peaks and valleys and the deviation from the mean line on the entire surface within the sampling length. Ra averages all peaks and valleys of the roughness profile.
[5] Rz is the average maximum peak to valley of five consecutive sampling lengths within the measuring length.

To quantify the depth of sandblasting, i.e. affected the area, SECM data along with the micro-hardness profiles on the cross-section of the as received and sandblasted specimens are presented in Fig. 5.4. For all specimens, the current value at the surface of each specimen was higher compared to the other parts of the same specimen, due to the higher corrosion activity of the surface compared to the rest of the specimen. This observation corresponded well with the change in the microhardness versus the distance from the surface, which decreases progressively due to a transitional plastic deformed region. Increasing the time of sandblasting, increased the current at the surface. This current gradually decayed by moving toward the center of the specimen. At a particular distance from the surface of each specimen, the current, as well as the hardness, became stable and did not change.

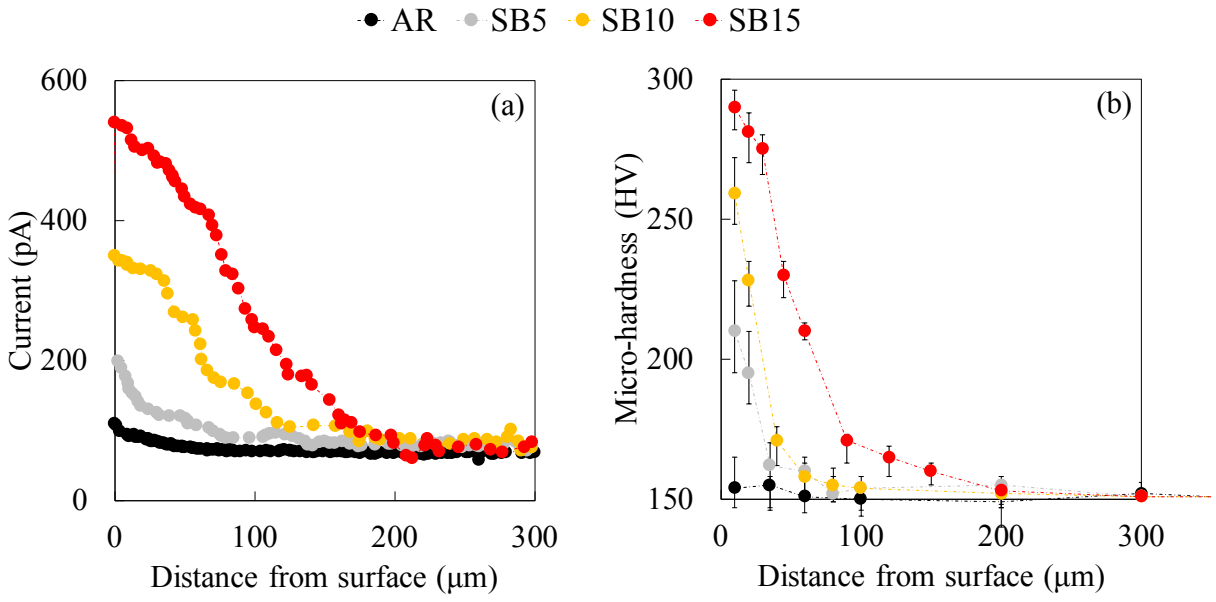

Figure 5. 4. (a) SECM currents obtained from the line scan, and (b) micro-hardness values from the cross-section of the specimens.

This distance was determined using the data from Fig. 5.4(a) and is shown in Fig. 5.5. As can be seen, there is a relatively linear relationship between this distance and the sandblasting time.

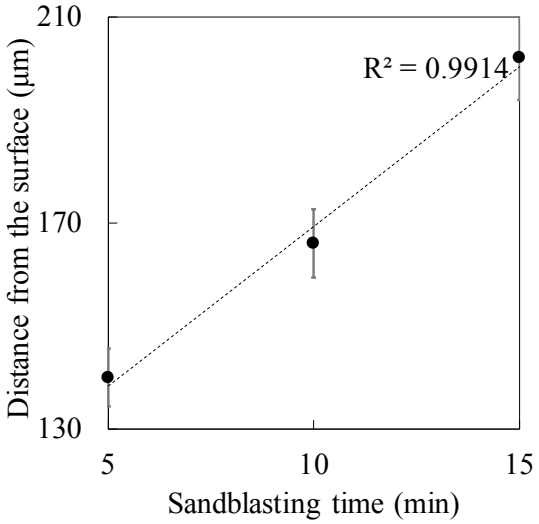

Figure 5. 5. Distance from the surface when the current stabilized in the SECM experiment.

This observation showed that sandblasting not only increased surface activity but also changed the electrochemical behavior of the bulk material by inducing plastic strain in the depth of material (Peyre, Scherpereel et al. 2000, Multigner, Frutos et al. 2009, Azar, Hashemi et al. 2010, Liu, Jin et al. 2015, Gatey, Hosmani et al. 2016). This change was linearly a function of the sandblasting time. Increasing current particularly at the surface due to sandblasting attributed to the refined structured layer with various dislocation configurations such as dense dislocation walls, dislocation tangles, and dislocation cells

(Liu, Lu et al. 2000, Dai, Villegas et al. 2004, Lu and Lu 2004, Balusamy, Kumar et al. 2010).

Fig. 5.6 shows the corrosion potential values of all specimens in all solutions. In a neutral solution, the SB5 specimens showed relatively nobler corrosion potential compared to the other specimens, followed by the as-received, SB10, and SB15. By the addition of the chlorides, all corrosion potential values shifted rapidly to more negative values which indicating increasing the corrosion activity. The corrosion potential values for all specimens became relatively stable after 2–3 days. However, the SB5 specimens still showed more positive indicating relatively less corrosion tendency compared to the other specimens. This observation for SB10 and SB15 was attributed to inducing micro-strains, reducing electron work function and decreasing the energy barrier for electrochemical reactions due to sandblasting (Wang, Yu et al. 2006, Mordyuk, Prokopenko et al. 2007, Hamu, Eliezer et al. 2009, Lee, Kim et al. 2009, Trdan and Grum 2012).

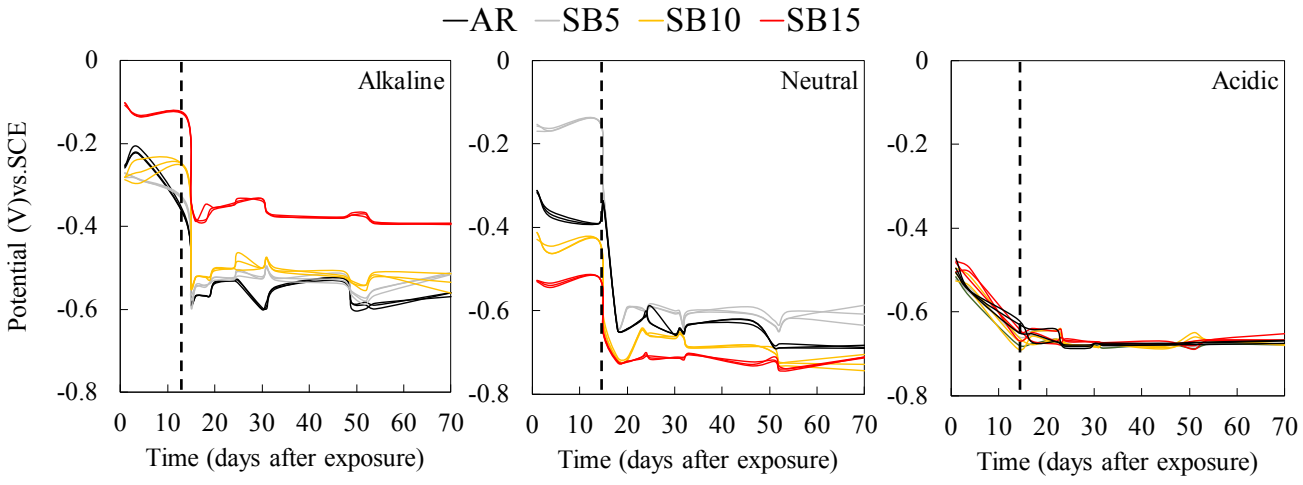

Figure 5. 6. Corrosion potential of values all specimens versus time of exposure. Vertical dashed lines represent the date of the addition of chlorides.

In chloride-free acidic solution, all specimens showed active corrosion and they had relatively similar potentials. These values shifted slightly to more negative values by the time of immersion, implying the anodic dissolution of the surface. Addition of chlorides did not affect the potential values significantly compare to a neutral solution, implying specimens corroded actively through the whole experiment.

In alkaline solution, the potential values showed the formation of the protective layer on the surface of the specimens in chloride-free solution (Dai, Villegas et al. 2004, Lu and Lu 2004, Figueira, Silva et al. 2015, Poursaee 2016, Rudawska, Danczak et al. 2016, Pour-Ali, Kiani-Rashid et al. 2017). The potential of the specimens in chloride-free alkaline solution was a function of sandblasting duration, i.e. increasing the time of sandblasting, shifted the potentials to more noble values. Addition of chlorides to the alkaline solution after 14 days shifted the corrosion potential values of AR, SB5 and SB10 specimens from −0.3 V to approximately −0.6 V vs. SCE, indicating the initiation and progress of dissolution, i.e. active corrosion, of those specimens. Nevertheless, the addition of chlorides altered the potential of SB15 from approximately −0.1 V to −0.4 V indicating less corrosion tendency, presumably due to the formation of a more ablative barrier layer on the surface of SB15 specimens compared to the other specimens (Jayalakshmi, Huilgol et al. 2016).

The corrosion current density values calculated from the results of the PLPR tests are shown in Fig. 5.7.

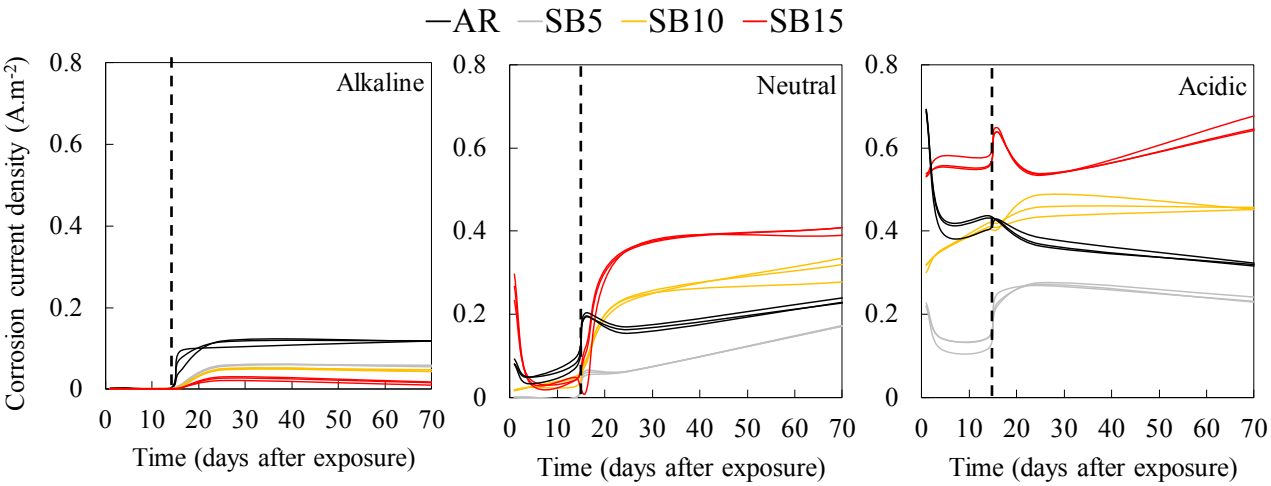

Figure 5. 7. Corrosion current densities of all specimen versus time of exposure. The vertical dashed line represents the date of the addition of chlorides.

In alkaline solution, all values of current densities were around 10^{-3} A·m^{-2} in chloride-free solution, indicating the formation of the protective layer on the surface of all specimens (Hansson 1984, Ding and Poursaee 2017). After addition of chlorides, the current densities of all specimens started to increase and reached to steady state after 4–5 days. This increment in corrosion activity, due to the addition of chloride, was highest for the AR specimens compared to the SB specimens and followed by SB15, SB10, and SB5 specimens. Obviously, the sandblasting improved the corrosion resistance of the steel in alkaline solution significantly. The results corresponded well with the results from the corrosion potential measurements. In contrast to the alkaline solution, in neutral and acidic solution, SB15 and then SB10 showed the highest corrosion current density, followed by as-received specimens, both before and after addition of chloride; and the SB5 specimens showed the lowest corrosion current density among the other specimens. In acidic solution, the addition of chloride did not noticeably change the corrosion current density of the

specimens, particularly for SB15 and SB10, compared to the neutral and alkaline solutions. While the result from the LPR indicated that the lowest corrosion activity for the SB5 specimens in acidic solution, the results of the corrosion potential measurements did not show this distinction.

The mass losses for all three specimens from each condition were calculated using the area under the curves (in Fig. 5.7) and Faraday's law (Poursaee 2011), and the percentages of the mass loss change of the sandblasted specimens versus the as-received specimens are shown in Fig. 5.8.

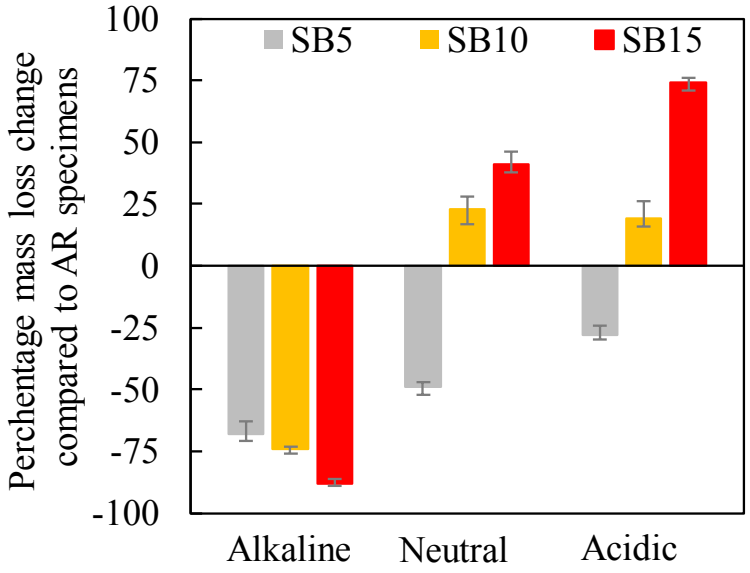

Figure 5. 8. Percentage of mass loss of the sandblasted specimens compared to the as-received specimens in different solutions during immersion.

The major change in corrosion resistance because of sandblasting occurred in alkaline solution. This change (improvement) was proportional with the time of sandblasting, i.e.

15 min sandblasting reduced the mass loss of the steel in alkaline solution compared to the as-received steel in the same solution, approximately 89%. However, in neutral and acidic solutions, 15 min sandblasting increased the mass loss of steel about 40 and 75%, respectively.

Fig. 5.9 shows the results of the cyclic polarization experiments on one of the specimens of each group 56 days after the addition of salt to the solutions.

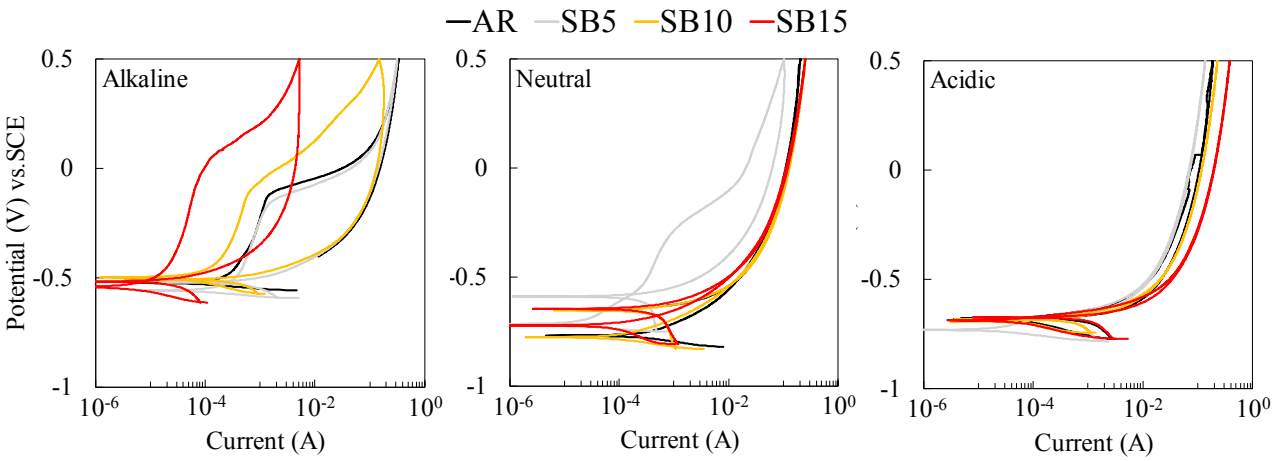

Figure 5. 9. Cyclic polarization curves of one of the specimens in each measurement cell 56 days after exposure to the chloride-contaminated solutions.

All specimens in neutral and acidic solutions showed active corrosion. The SB5 specimen in both neutral and acidic solution, particularly in the neutral solution, performed better compared to the other specimens which is in agreement with PLPR results. However, in alkaline solution, the SB15 specimen indicated lower active corrosion and higher pitting potential than the SB10, followed by the SB5 and the AR specimens. As we showed in SECM and PLPR part, longer sandblasted specimens showed more activity on the surface

which leads more oxidation preferably on defects or dislocations and grain bounders, however, in a high alkaline environment, this reaction with hydroxyl ions forms a passivating film on the iron surface. Therefore, a higher rate of reactions and rapid formation of Fe oxyhydroxide layer on a more defected matrix which acted as nucleation site improved passivation procedure (Afshari and Dehghanian 2009, Li, Hou et al. 2017). Comparing all polarization curves of the sandblasted specimens indicated that increasing the time of treatment increased the pitting potential which showed higher integrity of the passive layer for sandblasted specimens. This trend also can be seen in the reverse scan, where SB15 still maintained the lower passivation current.

In order to evaluate the effect of inducing plastic strain with sandblasting procedure on the corrosion and stability of corrosion film, impedance test was also performed. The Nyquist plots from the EIS tests, which are shown in Fig. 5.10, also indicated similar trends as the other electrochemical measurements. Each Nyquist plot was dominated by a capacitive arc. In alkaline solution, the SB15 specimens showed the highest corrosion resistance which corroborates with previous results. In the neutral and acidic solutions, the arc diameters for the SB5 were larger than others both before and after the addition of the chlorides.

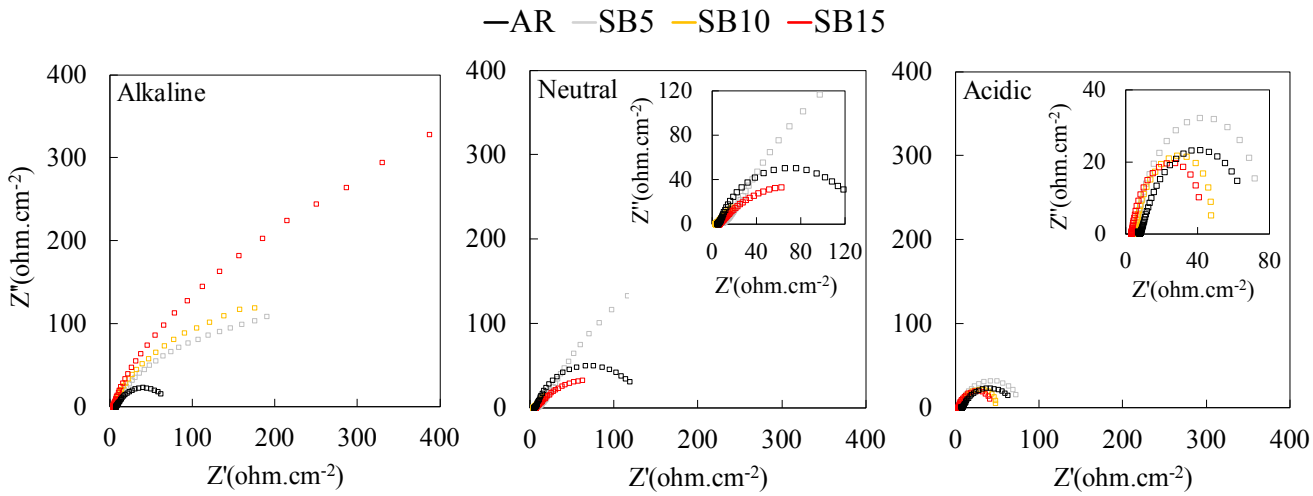

Figure 5. 10. Nyquist plots for one of the specimens in each measurement cell 8 weeks after exposure to the chloride-contaminated solutions.

All EIS data were fitted using the equivalent circuit shown in Fig. 5.11, where Rs was the solution resistance, Rpo was the resistance and CPEpo was the constant-phase element of the pores film, Rct was the charge-transfer resistance, and CPE_{dl} was the constant-phase element of double-layer.

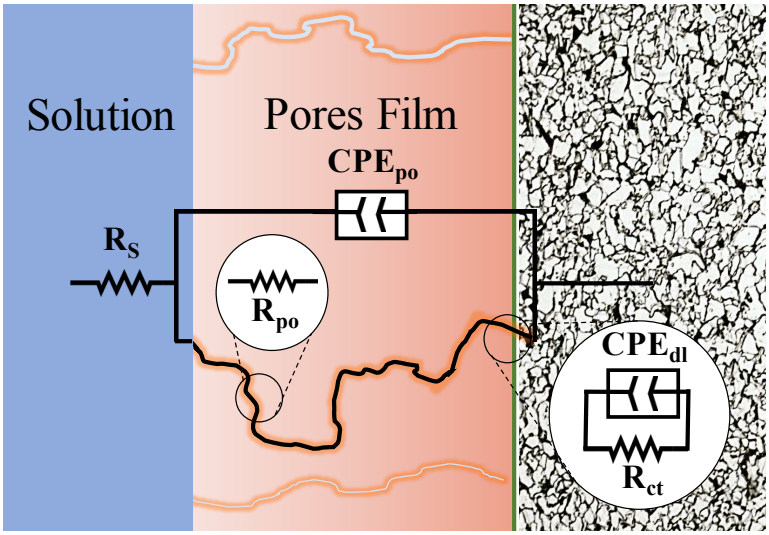

Figure 5. 11. Electrochemical equivalent circuits used to fit the EIS data in this work.

In the analysis of the Nyquist diagrams the constant phase element, CPE was used instead of an 'ideal' capacitor to address the deviations of the capacitive loops. The impedance, Z_{CPE} of the CPE, is described by the expression (Chintapalli, Rodriguez et al. 2014):

$$Z_{CPE} = [CPE(j\omega)^n]^{-1} \quad (5.1)$$

Where $j = \sqrt{-1}$, ω is angular frequency and n is deviation parameter, implying microscopic fluctuation of the surface metal, due to the surface heterogeneities (Raykowski, Hader et al. 2001, Chintapalli, Rodriguez et al. 2014). Depending on n, CPE can represent a pure capacitance (n=1) or a pure resistance (n=0). The deviation of n from these values indicates a deviation from the ideal behavior of the system, which was observed for all the specimens. The deviation from a pure capacitance behavior of the double-layer ascribed to surface heterogeneities at the micrometric (roughness, polycrystalline structure) and atomic (surface disorder as dislocations and steps, chemical in-homogeneities) scale and adsorption phenomena. The n_{po} values of less than 1, was attributed to the surface heterogeneities (Jorcin, Orazem et al. 2006, Córdoba-Torres, Mesquita et al. 2012).

The parameters obtained from a circuit equivalent are given in Table 5.2 for 56 days in chloride-contaminated solutions. It was shown that the values of the double-layer constant phase element capacitance are inversely proportional to the thickness of the passive layer (Geng, Sun et al. 2015). In alkaline solution, by increasing the time of sandblasting, R_{ct} and Rpo increases and double layer capacitance decreased, which indicates an increase in the thicker and smooth nature of protective layer forms on the surface of sandblasted

specimens. However, n values decreased by the time of sandblasting. Increasing the surface energy and the roughness of the sandblasted specimens could be the reason for such behavior.

Table 5. 2. Values of the elements of the equivalent circuit in Figure 5.11 to fit the impedance spectra of Figure 5.10.

Solution	Specimens	R_s	R_{ct}	R_{po}	CPE_{dl}	CPE_{po}	n_{dl}	n_{po}
		($\Omega.cm^2$)			($\Omega^{-1} s^n cm^{-2}$)			
Neutral	SB5	8.64	82.34	86.43	32.56	33.15	0.88	0.89
	SB10	9.56	73.42	77.25	56.18	34.17	0.95	0.93
	SB15	11.45	50.13	50.45	66.43	53.47	0.97	0.97
	AR	9.13	82.34	80.01	43.19	34.68	0.92	0.93
Acidic	SB5	12.01	31.01	35.12	125.68	118.09	0.91	0.91
	SB10	12.33	20.29	32.10	130.57	110.13	0.98	0.98
	SB15	12.29	15.03	11.03	213.12	290.03	0.98	0.98
	AR	12.16	27.68	30.19	112.40	112	0.92	0.92
Alkaline	SB5	7.79	106.56	116.31	21.31	16.32	0.82	0.82
	SB10	6.42	132.53	173.65	17.54	15.23	0.84	0.88
	SB15	5.38	279.35	283.42	10.43	18.65	0.80	0.85
	AR	8.63	76.40	82.69	32.53	32.05	0.85	0.86

In neutral and acidic solutions, the trends exactly complied with the other results, i.e. SB5 had the highest Rct values followed by the AR, SB10, and SB15. SB5 had the least capacitance meaning that the oxide layer formed on the surface was smooth and thicker compared to the other specimens even AR.

The enhanced corrosion resistance of the SB5 specimens compared to the SB10 and SB15 in neutral and acidic environments was attributed to the thickness of the affected layer. It

was hypothesized that due to the presence of rougher and more active layer (affected area) on the surface of the SB specimens, corrosion started and progressed with higher rates compared to the AR specimens, at the first stages of the immersion. This initiation and propagation was a function of sandblasting time, as demonstrated in SECM results. However, the thickness of the active affected area in the SB5 specimens was smaller, compared to the other sandblasted specimens. The microscopic analysis showed that the grain size in the SB5 specimens was about the same size as the thickness of the deformed area (Fig. 5.5 and Table 5.1). Thus, it was assumed that the 5 min sandblasting was not sufficient time to completely reform and induce micro-strain to deeper grains and, therefore, approximately the first series of surface grains were affected. Hence, due to the more active nature of the deformed grains compared to the other in-depth grains (Fig. 5.4a), at the first stages of the exposure, oxides layer were formed on the surface of the SB5 specimens faster than the AR specimens. By consuming, reacting and forming a layer from the surface grains, remained grains underneath of the SB5 specimens behaved similar to the AR specimens (less active) but with a layer of dense corrosion products on their surface. Similar behavior for the SB5 and AR specimens can be observed in Fig. 5.7 for neutral and acidic solutions. Furthermore, the Rpo for SB5 specimens in both neutral and acidic solutions were higher than those for the AR specimens. For the SB10 and SB15 specimens, however, the thicker affected area continued to corrode with high rate compared to the AR specimens.

5.4. Summary

This chapter aimed to study the influence of time of sandblasting, as a surface mechanical attrition treatment method, on the corrosion behavior of carbon steel in different solutions with different pHs. Optical microscopy, micro-hardness test, as well as Scanning Electrochemical Microscopy, were used to examine the affected area underneath the surface of the sandblasted specimens. The results of the electrochemical experiments showed significant improvement in corrosion resistance of the sandblasted specimens in the high alkaline solution. In neutral and acidic solutions, specimens sandblasted for 5 min showed superior corrosion resistance compared to the as-received and other specimens, sandblasted for a longer period of time.

In summary, it is found that:

1. SECM was successfully used to directly evaluate the impact of sandblasting as a simple example of SMAT process on the electrochemical activity of the steel surface in solution with neutral pH. This approach provided a better understanding of the effect of grain refinement and plastic deformation on the electrochemical behavior which corroborated well with micro-hardness data.
2. Sandblasting increased the surface roughness and induced plastic deformation within the depth of the steel. Increasing the duration of sandblasting, increased the thickness of the affected area. However, on average, the surface roughness (Ra) was not a function of the duration of the sandblasting.
3. SB5 specimens showed improved corrosion resistance compared to the other sandblasted (sandblasted for a longer period of time) and AR specimens in neutral

and acidic solutions. It was hypothesized that upon exposure to the neutral and acidic solutions, for the SB5 specimens, the affected area corroded rapidly, and corrosion products could act as a protective barrier and reduced the corrosion rate on the SB5 specimens. Nevertheless, the corrosion continued activity on the other SB specimens.

4. Sandblasted specimens showed more active corrosion compared to the as-received specimens in neutral and acidic solutions due to the high-energetic and strained areas formed by the impact of blasted sand. This increase in corrosion activity was the function of the time of sandblasting.
5. In alkaline solution, the formation of a presumably protective passive layer on the surface of the sandblasted specimens improved the corrosion resistance and enhanced integrity to the localized attack of these specimens. The improvement was proportional to the duration of sandblasting.

CHAPTER 6

6.CONCLUSIONS AND RECOMMENDATIONS

6.1. Conclusions

- In general, (except soil 8) the steel-mortar specimens and as-received specimens showed comparable corrosion activities in both as-received soils and soils with elevated chloride content.
- As-received steel specimens in as-received soil 3 showed the highest corrosion current densities less than 0.6 $A.m^{-2}$ compared to other as-received specimens.
- When chlorides were added, the steel-mortar specimens in soils 8 and 9 showed higher corrosion current densities compared to the other specimens.
- Corrosion potential values of all specimens remained relatively stable, both before and after the addition of chlorides, while the corrosion current densities were increased after the addition of the chlorides. Thus, based on this result, measuring just the corrosion potential was not an efficient and accurate method to evaluate the corrosion behavior of the steel in the soil.
- After measuring the actual corroded areas on each specimen, the results of the current density measurements were significantly changed.
- The physiochemical parameters available for the soils could not be used to explain the observed behaviors. It was hypothesized that the synergistic activity of the chlorides and SRB was the reason for a significant increase in the corrosion rates

of steel in soil 9. However, no information was available on the type and population of the bacteria in the soils to support this hypothesis.

- The galvanic corrosion was also observed between steel in soils with the same chemistry but different chloride contents.
- Sandblasting significantly enhanced the corrosion resistance of the steel in soil compared to as-received specimens.
- Old steel specimens retrieved from the bridge showed higher corrosion activity ($0.3 A.m^{-2}$) compared to the new as-received steel ($0.1 A.m^{-2}$). This point needs to be considered during repair and maintenance if such combination is expected.
- A very good correlation between the corrosion potential values and corrosion current densities obtained from the GRNN model and the experimental measurements was observed for the as-received soils. The sensitivity analysis was conducted on two input parameters, i.e. chloride content and moisture content. Results showed that changing these parameters had a significant impact on the corrosion current densities and corrosion potential values of the steel specimens. The chloride content of the as-received soils increased and the original model was run. Results showed that while the initial model could predict the corrosion activity of the steel specimens, the accuracy of the prediction was not very high ($R^2=0.60$). The model was trained again and the performance of the new model in predicting the corrosion activity of the steel in the soils with elevated chloride content was enhanced significantly ($R^2>0.88$).

- The model was used to predict the corrosion current densities and corrosion potential values of the steel specimens ahead of the actual experimental measurements and the results showed that the model is highly capable of predicting these values.
- To develop this model, the data from soils collected from different areas in the state of Wisconsin were used. The authors tried to establish a methodology in predicting corrosion of steel in the soil. Using the extensive body of data available at the NBS will admittedly enhance the model, which is currently under investigation and the results will be reported soon.
- SECM was successfully used to directly evaluate the impact of sandblasting as a simple example of SMAT process on the electrochemical activity of the steel surface in solution with neutral pH. This approach provided a better understanding of the effect of grain refinement and plastic deformation on the electrochemical behavior which corroborated well with micro-hardness data.
- Sandblasting increased the surface roughness and induced plastic deformation within the depth of the steel. Increasing the duration of sandblasting, increased the thickness of the affected area. However, on average, the surface roughness (Ra) was not a function of the duration of the sandblasting.
- SB5 specimens showed improved corrosion resistance compared to the other sandblasted (sandblasted for a longer period of time) and AR specimens in neutral and acidic solutions. It was hypothesized that upon exposure to the neutral and acidic solutions, for the SB5 specimens, the affected area corroded rapidly, and

corrosion products could act as a protective barrier and reduced the corrosion rate on the SB5 specimens. Nevertheless, the corrosion continued activity on the other SB specimens.

- Sandblasted specimens showed more active corrosion compared to the as-received specimens in neutral and acidic solutions due to the high-energetic and strained areas formed by the impact of blasted sand. This increase in corrosion activity was the function of the time of sandblasting.
- In alkaline solution, the formation of a presumably protective passive layer on the surface of the sandblasted specimens improved the corrosion resistance and enhanced integrity to the localized attack of these specimens. The improvement was proportional to the duration of sandblasting.

6.2. Recommendations

To further expand the work presented in this dissertation, a number of research topics may be undertaken, which include the following:

1. Further investigation of bacterial in all soils is suggested, such that the microbially induced corrosion can be more accurate included.
2. Other than the variables that considered in chapter 3 and chapter 4, the depth of soil is also a parameter worth considering.

3. For developing the GRNN model, using the extensive body of data available at the NBS will admittedly enhance the model, which is currently under investigation and the results will be reported soon.

APPENDIX A

PICTURES OF THE CORRODED SPECIMENS

As-received soil (with no Cl addition)/as-received steel

Soil 1

Specimen 1	
Side A	
Side B	

Specimen 2	
Side A	
Side B	

Specimen 3	
Side A	
Side B	

Soil 2

Specimen 1	
Side A	
Side B	

Specimen 2	
Side A	
Side B	

Specimen 3	
Side A	
Side B	

Soil 3

Specimen 1	
Side A	
Side B	

Specimen 2	
Side A	
Side B	

Specimen 3	
Side A	
Side B	

Soil 4

Specimen 1	
Side A	
Side B	

Specimen 2	
Side A	
Side B	

Specimen 3	
Side A	
Side B	

Soil 5

Specimen 1	
Side A	
Side B	

Specimen 2	
Side A	
Side B	

Specimen 3	
Side A	
Side B	

Soil 6

Specimen 1	
Side A	
Side B	

Specimen 2	
Side A	
Side B	

Specimen 3	
Side A	
Side B	

Soil 7

Specimen 1	
Side A	
Side B	

Specimen 2	
Side A	
Side B	

Specimen 3	
Side A	
Side B	

Soil 8

Specimen 1	
Side A	
Side B	

Specimen 2	
Side A	
Side B	

Specimen 3	
Side A	
Side B	

Soil 9

Specimen 1	
Side A	
Side B	

Specimen 2	
Side A	
Side B	

Specimen 3	
Side A	
Side B	

As-received soil (with no Cl addition)/ steel-mortar

Soil 1

Specimen 1	
Side A	
Side B	

Specimen 2	
Side A	
Side B	

Specimen 3	
Side A	
Side B	

Soil 2

Specimen 1	
Side A	
Side B	

Specimen 2	
Side A	
Side B	

Specimen 3	
Side A	
Side B	

Soil 3

Specimen 1	
Side A	
Side B	

Specimen 2	
Side A	
Side B	

Specimen 3	
Side A	
Side B	

Soil 4

Specimen 1	
Side A	
Side B	

Specimen 2	
Side A	
Side B	

Specimen 3	
Side A	
Side B	

Soil 5

Specimen 1	
Side A	
Side B	

Specimen 2	
Side A	
Side B	

Specimen 3	
Side A	
Side B	

Soil 6

Specimen 1	
Side A	
Side B	

Specimen 2	
Side A	
Side B	

Specimen 3	
Side A	
Side B	

Soil 7

Specimen 1	
Side A	
Side B	

Specimen 2	
Side A	
Side B	

Specimen 3	
Side A	
Side B	

Soil 8

Specimen 1	
Side A	
Side B	

Specimen 2	
Side A	
Side B	

Specimen 3	
Side A	
Side B	

Soil 9

Specimen 1	
Side A	
Side B	

Specimen 2	
Side A	
Side B	

Specimen 3	
Side A	
Side B	

Soil with Cl addition/as-received steel

Soil 1

Specimen 1	
Side A	
Side B	

Specimen 2	
Side A	
Side B	

Specimen 3	
Side A	
Side B	

Soil 2

Specimen 1	
Side A	
Side B	

Specimen 2	
Side A	
Side B	

Specimen 3	
Side A	
Side B	

Soil 3

Specimen 1	
Side A	
Side B	

Specimen 2	
Side A	
Side B	

Specimen 3	
Side A	
Side B	

Soil 4

Specimen 1	
Side A	
Side B	

Specimen 2	
Side A	
Side B	

Specimen 3	
Side A	
Side B	

Soil 5

Specimen 1	
Side A	
Side B	

Specimen 2	
Side A	
Side B	

Specimen 3	
Side A	
Side B	

Soil 6

Specimen 1	
Side A	
Side B	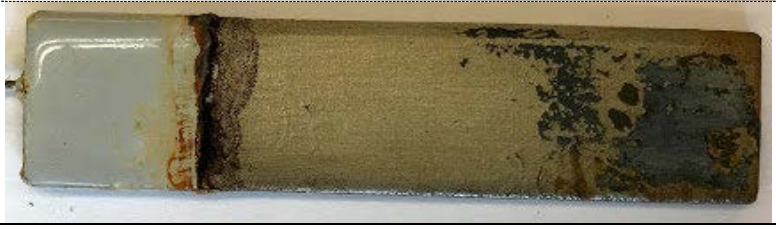

Specimen 2	
Side A	
Side B	

Specimen 3	
Side A	
Side B	

Soil 7

Specimen 1	
Side A	
Side B	

Specimen 2	
Side A	
Side B	

Specimen 3	
Side A	
Side B	

Soil 8

Specimen 1	
Side A	
Side B	

Specimen 2	
Side A	
Side B	

Specimen 3	
Side A	
Side B	

Soil 9

Specimen 1	
Side A	
Side B	

Specimen 2	
Side A	
Side B	

Specimen 3	
Side A	
Side B	

Soil with Cl addition/ steel-mortar

Soil 1

Specimen 1	
Side A	
Side B	

Specimen 2	
Side A	
Side B	

Specimen 3	
Side A	
Side B	

Soil 2

Specimen 1	
Side A	
Side B	

Specimen 2	
Side A	
Side B	

Specimen 3	
Side A	
Side B	

Soil 3

Specimen 1	
Side A	
Side B	

Specimen 2	
Side A	
Side B	

Specimen 3	
Side A	
Side B	

Soil 4

Specimen 1	
Side A	
Side B	

Specimen 2	
Side A	
Side B	

Specimen 3	
Side A	
Side B	

Soil 5

Specimen 1	
Side A	
Side B	

Specimen 2	
Side A	
Side B	

Specimen 3	
Side A	
Side B	

Soil 6

Specimen 1	
Side A	
Side B	

Specimen 2	
Side A	
Side B	

Specimen 3	
Side A	
Side B	

Soil 7

Specimen 1	
Side A	
Side B	

Specimen 2	
Side A	
Side B	

Specimen 3	
Side A	
Side B	

Soil 8

Specimen 1	
Side A	
Side B	

Specimen 2	
Side A	
Side B	

Specimen 3	
Side A	
Side B	

Soil 9

Specimen 1	
Side A	
Side B	

Specimen 2	
Side A	
Side B	

Specimen 3	
Side A	
Side B	

REFERENCES:

ImageJ. National Institutes of Health, http://rsbweb.nih.gov/ij/.

Afshari, V. and C. Dehghanian (2009). "Effects of grain size on the electrochemical corrosion behaviour of electrodeposited nanocrystalline Fe coatings in alkaline solution." Corrosion Science **51**(8): 1844-1849.

Amanov, A. and Y.-S. Pyun (2017). "Local heat treatment with and without ultrasonic nanocrystal surface modification of Ti-6Al-4V alloy: Mechanical and tribological properties." Surface and Coatings Technology **326**: 343-354.

An, Y.-L., et al. (2013). "Interfacial structure and mechanical properties of surface iron–nickel alloying layer in pure iron fabricated by surface mechanical attrition alloy treatment." Materials & Design **46**: 627-633.

Astaraee, A. H., et al. (2017). "Incorporating the principles of shot peening for a better understanding of surface mechanical attrition treatment (SMAT) by simulations and experiments." Materials & Design **116**: 365-373.

ASTM (2000). ASTM D2974-87, standard test method for moisture,ash, and organic matter of peat and other organic soils., ASTM International.

ASTM (2004). G5-94: Standard Reference Test Method for Making Potentiostatic and Potentiodynamic Anodic Polarization Measurements, ASTM.

Azar, V., et al. (2010). "The effect of shot peening on fatigue and corrosion behavior of 316L stainless steel in Ringer's solution." Surface and Coatings Technology **204**(21-22): 3546-3551.

Bagherifard, S., et al. (2016). "Nanoscale surface modification of AISI 316L stainless steel by severe shot peening." Materials & Design **102**: 68-77.

Balusamy, T., et al. (2010). "Effect of surface nanocrystallization on the corrosion behaviour of AISI 409 stainless steel." Corrosion Science **52**(11): 3826-3834.

Beben, D. (2014). "Backfill Corrosivity around Corrugated Steel Plate Culverts." Journal of Performance of Constructed Facilities **29**(6): 04014159.

Becker, S. and K. Rudat (2014). "I-43 Leo Frigo Memorial Bridge Investigation Report - Draft Executive Summary." (Wisconsin Department of Transportation).

Benafia, S., et al. (2018). "Influence of Surface Mechanical Attrition Treatment on the oxidation behaviour of 316L stainless steel." Corrosion Science.

Benmoussat, A. and M. Hadjel (2005). "Corrosion behavior of low carbon line pipe steel in soil environment." J Corros Sci Eng **7**: 14.

Bentur, A., et al. (1997). Steel corrosion in concrete: fundamentals and civil engineering practice, CRC Press.

Cai, J., et al. (1999). "Phenomenological modelling of atmospheric corrosion using an artificial neural network." Corrosion Science **41**(10): 2001-2030.

Chaker, V. (1989). Effects of soil characteristics on corrosion, ASTM International.

Chatterjee, A., et al. (2009). "Evaluation of different soil carbon determination methods." Critical Reviews in Plant Science **28**(3): 164-178.

Chen, A., et al. (2013). "The influence of interface structure on nanocrystalline deformation of a layered and nanostructured steel." Materials & Design **47**: 316-322.

Chen, T., et al. (2013). "Influence of surface modifications on pitting corrosion behavior of nickel-base alloy 718. Part 1: Effect of machine hammer peening." Corrosion Science **77**: 230-245.

Chen, X., et al. (2005). "Tensile properties of a nanocrystalline 316L austenitic stainless steel." Scripta Materialia **52**(10): 1039-1044.

Chintapalli, R. K., et al. (2013). "Phase transformation and subsurface damage in 3Y-TZP after sandblasting." Dental Materials **29**(5): 566-572.

Chintapalli, R. K., et al. (2014). "Effect of sandblasting and residual stress on strength of zirconia for restorative dentistry applications." Journal of the mechanical behavior of biomedical materials **29**: 126-137.

Cole, I. and D. Marney (2012). "The science of pipe corrosion: A review of the literature on the corrosion of ferrous metals in soils." Corrosion Science **56**: 5-16.

Córdoba-Torres, P., et al. (2012). "On the intrinsic coupling between constant-phase element parameters α and Q in electrochemical impedance spectroscopy." Electrochimica acta **72**: 172-178.

Costerton, J. W., et al. (1987). "Bacterial biofilms in nature and disease." Annual Reviews in Microbiology **41**(1): 435-464.

Cottis, R., et al. (1999). "Neural network methods for corrosion data reduction." Materials & Design **20**(4): 169-178.

Dai, K., et al. (2004). "Finite element modeling of the surface roughness of 5052 Al alloy subjected to a surface severe plastic deformation process." Acta materialia **52**(20): 5771-5782.

Decker, J. B., et al. (2008). "Corrosion rate evaluation and prediction for piles based on long-term field performance." Journal of geotechnical and geoenvironmental engineering **134**(3): 341-351.

Denison, I. and R. Hobbs (1934). "Corrosion of ferrous metals in acid soils." J. Res., National Bureau of Standards **13**: 125.

Ding, L. and A. Poursaee (2017). "The impact of sandblasting as a surface modification method on the corrosion behavior of steels in simulated concrete pore solution." Construction and Building Materials **157**: 591-599.

Doyle, G., et al. (2003). "The role of soil in the external corrosion of cast iron water mains in Toronto, Canada." Canadian geotechnical journal **40**(2): 225-236.

Elias, V. and B. R. Christopher (1997). Mechanically stabilized earthwalls and reinforced soil slopes, design and construction guidelines. Washington DC, Federal Highway Administration.

Enning, D., et al. (2012). "Marine sulfate-reducing bacteria cause serious corrosion of iron under electroconductive biogenic mineral crust." Environmental microbiology **14**(7): 1772-1787.

EPA (1982). "Method 120.1: Conductance (Specific Conductance, umhos at 25°C) by conductivity meter."

EPA (2004). "Method 9045D: Soil and waste pH."

EPA (2010). "Method 9060: Total Organic Carbon (TOC) in soil."

Fang, S., et al. (2008). "Hybrid genetic algorithms and support vector regression in forecasting atmospheric corrosion of metallic materials." Computational Materials Science **44**(2): 647-655.

Fauque, G. D. (1995). Ecology of sulfate-reducing bacteria. Sulfate-Reducing Bacteria, Springer**:** 217-241.

Feliu, S. and M. Morcillo (1993). "The prediction of atmospheric corrosion from meteorological and pollution parameters—I. Annual corrosion." Corrosion Science **34**(3): 403-414.

Ferreira, C. and J. Ponciano (2006). "Determination of the soil corrosivity of samples from southeastern Brazilian region." Eurocorr, Maastricht, Holland.

Ferreira, C. A. M., et al. (2007). "Evaluation of the corrosivity of the soil through its chemical composition." Science of the total environment **388**(1): 250-255.

Figueira, R. B., et al. (2015). "Hybrid sol–gel coatings for corrosion protection of hot-dip galvanized steel in alkaline medium." Surface and Coatings Technology **265**: 191-204.

Fitzgerald, J. (1993). "Evaluating soil corrosivity--Then and now." Materials Performance;(United States) **32**(10).

Fleming, K., et al. (2008). Piling engineering, CRC press.

Fonseca, I., et al. (2015). "Validation of the Steinrath Index Predictions for the Degree of Soil Aggressiveness Toward Copper Corrosion in Soils Contaminated with Chlorides." Corrosion **71**(10): 1267-1277.

Fontana, M. G. (2005). Corrosion engineering, Tata McGraw-Hill Education.

Fu, T., et al. (2015). "Effect of surface mechanical attrition treatment on corrosion resistance of commercial pure titanium." Surface and Coatings Technology **280**: 129-135.

Gatey, A. M., et al. (2016). "Role of surface mechanical attrition treatment and chemical etching on plasma nitriding behavior of AISI 304L steel." Surface and Coatings Technology **304**: 413-424.

Geng, S., et al. (2015). "Effect of sandblasting and subsequent acid pickling and passivation on the microstructure and corrosion behavior of 316L stainless steel." Materials & Design **88**: 1-7.

Graupe, D. (1972). Identification of systems, Van Nostrand Reinhold Company.

Gupta, S. and B. Gupta (1979). "The critical soil moisture content in the underground corrosion of mild steel." Corrosion Science **19**(3): 171-178.

Halim, A., et al. (2012). "Short term corrosion monitoring of carbon steel by bio-competitive exclusion of thermophilic sulphate reducing bacteria and nitrate reducing bacteria." Electrochimica acta **77**: 348-362.

Hamilton, W. A. (1985). "Sulphate-reducing bacteria and anaerobic corrosion." Annual Reviews in Microbiology **39**(1): 195-217.

Hamu, G. B., et al. (2009). "The relation between severe plastic deformation microstructure and corrosion behavior of AZ31 magnesium alloy." Journal of alloys and compounds **468**(1-2): 222-229.

Hansson, C. M. (1984). "Comments on electrochemical measurements of the rate of corrosion of steel in concrete." Cement and Concrete Research **14**(4): 574-584.

Hassani, S., et al. (2009). "Improving the corrosion and tribocorrosion resistance of Ni–Co nanocrystalline coatings in NaOH solution." Corrosion Science **51**(10): 2371-2379.

Hautman, D. P. and D. J. Munch (1997). "Method 300.1 Determination of inorganic anions in drinking water by ion chromatography." EPA: Ohio.

Haynie, F. and J. Upham (1974). Correlation between corrosion behavior of steel and atmospheric pollution data. Corrosion in Natural Environments, ASTM International.

Helliwell, I., et al. (1996). Neural networks for corrosion data reduction, NACE International, Houston, TX (United States).

Hertz, J., et al. (1991). Introduction to the theory of neural computation, Basic Books.

Hou, J., et al. (1997). "Improving both bond strength and corrosion resistance of steel rebar in concrete by water immersion or sand blasting of rebar." Cement and Concrete Research **27**(5): 679-684.

Hou, J., et al. (2011). "Effects of cold working degrees on grain boundary characters and strain concentration at grain boundaries in Alloy 600." Corrosion Science **53**(3): 1137-1142.

Hou, W. (1993). "ATMOSPHERIC CORROSION OF CARBON STEELS AND LOW ALLOY STEELS(Chinese)." J. Chinese Soc. of Corrosion and Protection **13**(4): 291-302.

Hubert, C., et al. (2005). "Corrosion risk associated with microbial souring control using nitrate or nitrite." Applied Microbiology and Biotechnology **68**(2): 272-282.

Jack, T., et al. (1994). The Characterization of Sulfate-Reducing Bacteria in Heavy Oil Waterflood Operations. Microbiologically influenced corrosion testing, ASTM International.

Jančíková, Z., et al. (2008). "Rabljenje metode umjetne inteligencije za predmnijevanje mehaničkih svojstava čelika." Metalurgija **47**(4): 339-342.

Jančíková, Z., et al. (2013). "Prediction of metal corrosion by neural networks." Metalurgija **52**(3): 379-381.

Jang, J.-S. (1993). "ANFIS: adaptive-network-based fuzzy inference system." IEEE transactions on systems, man, and cybernetics **23**(3): 665-685.

Javaherdashti, R. (1999). "A review of some characteristics of MIC caused by sulfate-reducing bacteria: past, present and future." Anti-Corrosion Methods and Materials **46**(3): 173-180.

Javaherdashti, R. (2000). "A fuzzy approach to model RISK of MIC in a cathodically-protected pipe." Anti-Corrosion Methods and Materials **47**(3): 142-146.

Javaherdashti, R. (2011). "Impact of sulphate-reducing bacteria on the performance of engineering materials." Applied Microbiology and Biotechnology **91**(6): 1507.

Jayalakshmi, M., et al. (2016). "Microstructural characterization of low temperature plasma-nitrided 316L stainless steel surface with prior severe shot peening." Materials & Design **108**: 448-454.

Jorcin, J.-B., et al. (2006). "CPE analysis by local electrochemical impedance spectroscopy." Electrochimica acta **51**(8-9): 1473-1479.

Kartalopoulos, S. V. and S. V. Kartakapoulos (1997). Understanding neural networks and fuzzy logic: basic concepts and applications, Wiley-IEEE Press.

Lee, H.-S., et al. (2009). "Influence of peening on the corrosion properties of AISI 304 stainless steel." Corrosion Science **51**(12): 2826-2830.

Lee, W. and W. G. Characklis (1993). "Corrosion of mild steel under anaerobic biofilm." Corrosion **49**(3): 186-199.

Li, Y., et al. (2017). "Enhancement of siliconizing behaviors in pure iron induced by surface mechanical attrition treatment." Surface and Coatings Technology **309**: 462-470.

Lin, H.-M., et al. (2009). "Neural network-based model for assessing failure potential of highway slopes in the Alishan, Taiwan Area: Pre-and post-earthquake investigation." Engineering Geology **104**(3-4): 280-289.

Lin, Y. and G. A. Cunningham (1995). "A new approach to fuzzy-neural system modeling." IEEE Transactions on Fuzzy systems **3**(2): 190-198.

Little, B. B., et al. (2000). The Relationship Between Corrosion and the Biological Sulfur Cycle, NAVAL RESEARCH LAB STENNIS SPACE CENTER MS OCEANOGRAPHY DIV.

Liu, G., et al. (2000). "Surface nanocrystallization of 316L stainless steel induced by ultrasonic shot peening." Materials Science and Engineering: A **286**(1): 91-95.

Liu, G., et al. (2001). "Low carbon steel with nanostructured surface layer induced by high-energy shot peening." Scripta Materialia **44**(8): 1791-1795.

Liu, T., et al. (2010). "Effect of soil compositions on the electrochemical corrosion behavior of carbon steel in simulated soil solution. Einfluss der Erdbodenzusammensetzung auf das elektrochemische Verhalten von Kohlenstoffstählen in simulierten Erdbodenlösungen." Materialwissenschaft und Werkstofftechnik **41**(4): 228-233.

Liu, Y., et al. (2015). "Wear behavior of nanocrystalline structured magnesium alloy induced by surface mechanical attrition treatment." Surface and Coatings Technology **261**: 219-226.

Lu, K. and J. Lu (2004). "Nanostructured surface layer on metallic materials induced by surface mechanical attrition treatment." Materials Science and Engineering: A **375**: 38-45.

Marques, A., et al. (2015). "SECM imaging of the cut edge corrosion of galvanized steel as a function of pH." Electrochimica acta **153**: 238-245.

Moore, T. and C. Hallmark (1987). "Soil Properties Influencing Corrosion of Steel in Texas Soils 1." Soil science society of America journal **51**(5): 1250-1256.

Morcillo, M., et al. (1995). Long-term atmospheric corrosion in Spain: results after 13–16 years of exposure and comparison with worldwide data. Atmospheric Corrosion, ASTM International.

Morcous, G. and Z. Lounis (2005). "Prediction of Onset of Corrosion in Concrete Bridge Decks Using Neural Networks and Case-Based Reasoning." Computer-Aided Civil and Infrastructure Engineering **20**(2): 108-117.

Mordyuk, B., et al. (2007). "Effect of structure evolution induced by ultrasonic peening on the corrosion behavior of AISI-321 stainless steel." Materials Science and Engineering: A **458**(1-2): 253-261.

Mousavifard, S., et al. (2015). "Application of artificial neural network and adaptive neuro-fuzzy inference system to investigate corrosion rate of zirconium-based nano-

ceramic layer on galvanized steel in 3.5% NaCl solution." Journal of alloys and compounds **639**: 315-324.

Multigner, M., et al. (2010). "Superficial severe plastic deformation of 316 LVM stainless steel through grit blasting: Effects on its microstructure and subsurface mechanical properties." Surface and Coatings Technology **205**(7): 1830-1837.

Multigner, M., et al. (2009). "Influence of the sandblasting on the subsurface microstructure of 316LVM stainless steel: Implications on the magnetic and mechanical properties." Materials Science and Engineering: C **29**(4): 1357-1360.

Natke, H. G. (2014). Application of system identification in engineering, Springer.

Neaupane, K. M. and S. H. Achet (2004). "Use of backpropagation neural network for landslide monitoring: a case study in the higher Himalaya." Engineering Geology **74**(3-4): 213-226.

Noor, E. A. and A. H. Al-Moubaraki (2014). "Influence of soil moisture content on the corrosion behavior of X60 steel in different soils." Arabian Journal for Science and Engineering **39**(7): 5421-5435.

Novák, V., et al. (2012). Mathematical principles of fuzzy logic, Springer Science & Business Media.

Oldeman, L., et al. (1990). World map of the status of human-induced soil degradation: an explanatory note, International Soil Reference and Information Centre.

Oldfield, J. W. (1988). Electrochemical theory of galvanic corrosion. Galvanic Corrosion, ASTM International.

Palmer, J. D. (1989). Environmental characteristics controlling the soil corrosion of ferrous piping. Effects of soil characteristics on corrosion, ASTM International.

Parthiban, T., et al. (2005). "Neural network analysis for corrosion of steel in concrete." Corrosion Science **47**(7): 1625-1642.

Peabody, A. W. (1967). Control of pipeline corrosion, National Association of corrosion engineers Houston, Texas.

Penhale, H. (1984). "Corrosion of mild steel plates in some New Zealand soils, after 20 years." New Zealand journal of science.

Petan, L., et al. (2016). "Influence of laser shock peening pulse density and spot size on the surface integrity of X2NiCoMo18-9-5 maraging steel." Surface and Coatings Technology **307**: 262-270.

Peyre, P., et al. (2000). "Surface modifications induced in 316L steel by laser peening and shot-peening. Influence on pitting corrosion resistance." Materials Science and Engineering: A **280**(2): 294-302.

Pintos, S., et al. (2000). "Artificial neural network modeling of atmospheric corrosion in the MICAT project." Corrosion Science **42**(1): 35-52.

Pour-Ali, S., et al. (2017). "Surface nanocrystallization and gradient microstructural evolutions in the surface layers of 321 stainless steel alloy treated via severe shot peening." Vacuum **144**: 152-159.

Pour-Ali, S., et al. (2018). "Correlation between the surface coverage of severe shot peening and surface microstructural evolutions in AISI 321: A TEM, FE-SEM and GI-XRD study." Surface and Coatings Technology **334**: 461-470.

Poursaee, A. (2010). "Potentiostatic transient technique, a simple approach to estimate the corrosion current density and Stern–Geary constant of reinforcing steel in concrete." Cement and Concrete Research **40**: 1451–1458.

Poursaee, A. (2011). "Corrosion measurement techniques in steel reinforced concrete." Journal of ASTM International **8**(5): 1-15.

Poursaee, A. (2016). "Temperature dependence of the formation of the passivation layer on carbon steel in high alkaline environment of concrete pore solution." Electrochemistry Communications **73**: 24-28.

Pradhan, B. and S. Lee (2010). "Delineation of landslide hazard areas on Penang Island, Malaysia, by using frequency ratio, logistic regression, and artificial neural network models." Environmental Earth Sciences **60**(5): 1037-1054.

Pritchard, O., et al. (2013). "Soil corrosivity in the UK–Impacts on Critical Infrastructure." Infrastructure Transitions Research Consortium Working paper series: 1-55.

Railsback, S. F. and V. Grimm (2011). Agent-based and individual-based modeling: a practical introduction, Princeton university press.

Rajani, B. and J. Makar (2000). "A methodology to estimate remaining service life of grey cast iron water mains." Canadian Journal of Civil Engineering **27**(6): 1259-1272.

Raykowski, A., et al. (2001). "Blast cleaning of gas turbine components: deposit removal and substrate deformation." Wear **249**(1): 126-131.

Reiser, C. A., et al. (2005). "A reverse-current decay mechanism for fuel cells." Electrochemical and Solid-State Letters **8**(6): A273-A276.

Ricker, R. E. (2010). "Analysis of pipeline steel corrosion data from NBS (NIST) studies conducted between 1922–1940 and relevance to pipeline management." Journal of research of the National Institute of Standards and Technology **115**(5): 373.

Roberge, P. R. (2000). Handbook of corrosion engineering, McGraw-Hill.

Robinson, W. (1993). "Testing soil for corrosiveness." Materials Performance;(United States) **32**(4).

Romanoff, M. (1970). Performance of Steel Pilings in Soils. PAPER FROM PROC 25 TH CONF NAT ASSOC CORROS ENG, NACE, HOUSTON, TEX. 1970, 14-22.

Rosen, E. and D. Silverman (1992). "Corrosion prediction from polarization scans using an artificial neural network integrated with an expert system." Corrosion **48**(9): 734-745.

Rudawska, A., et al. (2016). "The effect of sandblasting on surface properties for adhesion." International Journal of Adhesion and Adhesives **70**: 176-190.

Saji, G. (2010). Radiation induced 'long-cell'(macrocell) corrosion in water-cooled reactors of Russian design. Material issues in design, manufacturing and operation of nuclear power plants equipment. In: 11th Prometey Int. Conf., St. Petersburg, Russia.

Sand, W. (1997). "Microbial mechanisms of deterioration of inorganic substrates—a general mechanistic overview." International biodeterioration & biodegradation **40**(2-4): 183-190.

Setareh, M. and R. Javaherdashti (2006). "Evaluation of sessile microorganisms in pipelines and cooling towers of some Iranian industries." Journal of Materials Engineering and Performance **15**(1): 5-8.

Shahin, M. A., et al. (2001). "Artificial neural network applications in geotechnical engineering." Australian geomechanics **36**(1): 49-62.

Singh, M. and T. Markeset (2009). "A methodology for risk-based inspection planning of oil and gas pipes based on fuzzy logic framework." Engineering Failure Analysis **16**(7): 2098-2113.

Smets, H. and W. Bogaerts (1992). "SCC analysis of austenitic stainless steels in chloride-bearing water by neural network techniques." Corrosion **48**(8): 618-623.

Smola, A. J. and B. Schölkopf (2004). "A tutorial on support vector regression." Statistics and computing **14**(3): 199-222.

Soil, A. C. D.-o. and Rock (2011). Standard practice for classification of soils for engineering purposes (Unified Soil Classification System), ASTM International.

Specht, D. F. (1991). "A general regression neural network." IEEE transactions on neural networks **2**(6): 568-576.

Sturrock, C. and W. Bogaerts (1997). "Empirical learning investigations of the stress corrosion cracking of austenitic stainless steels in high-temperature aqueous environments." Corrosion **53**(4): 333-343.

Sun, H., et al. (2008). "Surface alloying of an Mg alloy subjected to surface mechanical attrition treatment." Surface and Coatings Technology **202**(16): 3947-3953.

Sung, A. (1998). "Ranking importance of input parameters of neural networks." Expert Systems with Applications **15**(3-4): 405-411.

Sungur, E. I., et al. (2010). "Monitoring and disinfection of biofilm-associated sulfate reducing bacteria on different substrata in a simulated recirculating cooling tower system." Turkish Journal of Biology **34**(4): 389-397.

Tao, N., et al. (2002). "An investigation of surface nanocrystallization mechanism in Fe induced by surface mechanical attrition treatment." Acta materialia **50**(18): 4603-4616.

Tiller, K. (1950). "A REVIEW OF THE EUROPEAN RESEARCH EFFORT ON MICROBIAL CORROSION BETWEEN 1950 AND 1984 A."

Torbati-Sarraf, H. and A. Poursaee (2018). "Corrosion of coupled steels with different microstructures in concrete environment." Construction and Building Materials **167**: 680-687.

Trasatti, S. and F. Mazza (1996). "Crevice corrosion: a neural network approach." British Corrosion Journal **31**(2): 105-112.

Trdan, U. and J. Grum (2012). "Evaluation of corrosion resistance of AA6082-T651 aluminium alloy after laser shock peening by means of cyclic polarisation and ElS methods." Corrosion Science **59**: 324-333.

Trungesvik, K. (1976). Investigations of corrosion rates on steel piles in Norwegian marine sediments, Norwegian Geotechnical Institute.

Vapnik, V. (1995). "The nature of statistical learning theory Springer New York Google Scholar."

Videla, H. (1985). "Corrosion of Mild Steel Induced by Sulphate Reducing Bacteria--a Study of Passivity Breakdown by Biogenic Sulphides." Biologically induced corrosion: 162-170.

von Wolzogen Kuehr, C. and L. Van der Vlugt (1964). Graphitization of cast iron as an electrobiochemical process in anaerobic soils, ARMY BIOLOGICAL LABS FREDERICK MD.

Wang, H., et al. (2003). "Stainless steel as bipolar plate material for polymer electrolyte membrane fuel cells." Journal of Power Sources **115**(2): 243-251.

Wang, T., et al. (2006). "Surface nanocrystallization induced by shot peening and its effect on corrosion resistance of 1Cr18Ni9Ti stainless steel." Surface and Coatings Technology **200**(16-17): 4777-4781.

Wang, X. and D. Li (2002). "Mechanical and electrochemical behavior of nanocrystalline surface of 304 stainless steel." Electrochimica acta **47**(24): 3939-3947.

Wang, X., et al. Electrochemical Characterization of the Soils Surrounding Buried or Embedded Steel Elements. Pipelines 2016**:** 110-116.

Wang, X., et al. (2016). Electrochemical Characterization of the Soils Surrounding Buried or Embedded Steel Elements. Pipelines 110-116.

Wen, Y., et al. (2009). "Corrosion rate prediction of 3C steel under different seawater environment by using support vector regression." Corrosion Science **51**(2): 349-355.

Wong, I. (2001). "Methods of resisting hydrostatic uplift in substructures." Tunnelling and underground space technology **16**(2): 77-86.

Wong, I. H. and K. H. Law (1999). "Corrosion of steel H piles in decomposed granite." Journal of geotechnical and geoenvironmental engineering **125**(6): 529-532.

Yan, M., et al. (2014). "Role of Fe oxides in corrosion of pipeline steel in a red clay soil." Corrosion Science **80**: 309-317.

Yin, Z., et al. (2016). "Strength and ductility of gradient structured copper obtained by surface mechanical attrition treatment." Materials & Design **105**: 89-95.

Yuan, L., et al. (2015). "Enhancing the oxidation resistance of copper by using sandblasted copper surfaces." Applied Surface Science **357**: 2160-2168.